A NANOCHANNEL WITH AN EMBEDDED TRANSVERSE GRAPHENE TUNNELING ELECTRODE FOR MOLECULAR PROBING AND AS A FUTURE TOOL FOR DNA SEQUENCING

BY MANUEL SCHOTTDORF

A thesis submitted to the

Graduate School—New Brunswick

Rutgers, The State University of New Jersey

in partial fulfillment of the requirements

for the degree of

Master of Science

Graduate Program in Physics and Astronomy

Written under the direction of

Professor Eva Andrei

and approved by

_____

_____

_____

_____

New Brunswick, New Jersey

October, 2011

ABSTRACT OF THE THESIS

A nanochannel with an embedded transverse graphene tunneling electrode for molecular probing and as a future tool for DNA sequencing

by Manuel Schottdorf

Thesis Director: Professor Eva Andrei

Single layer graphene, as a one-atom-thick highly conductive layer, is an exciting candidate for highly localized tunneling measurements because it is sufficiently thin to resolve a single molecule. We have fabricated graphene tunneling junctions confined within a nanochannel to explore the feasibility of developing a single-molecule sequencing tool for deoxyribonucleic acid (DNA). The unprecedented thinness of graphene electrodes allows to overcome the problems encountered using metallic electrodes, which are too bulky for single-molecule resolution. By confining of the molecule in a nanochannel, a long and narrow structure through which it can be dragged electrophoretically, it is possible to slow down the DNA sufficiently to achieve single base translocation. We show an experimental realization of the first steps towards a new graphene sequencing device.

First, we present a new experimental technique for the production of nanogaps in a sheet of graphene. Applying a high current density in a graphene strip removes material from the strip resulting in the formation of nanogaps and tips. Starting from graphene grown by Chemical Vapor Deposition (CVD), we fabricate those structures. We show transport measurements of graphene devices in helium, air and vacuum demonstrating the

realization of tunneling gaps.

Second, we embed graphene tunneling junctions in a nanochannel and measure tunneling currents through various liquids. Using Simmons' model we calculate the work function between graphene and those liquids.

Third we present evidence for inelastic tunneling through different molecules especially Rhodamine B and Adenosine monophosphate. We compare the results with data from optical spectroscopy.

Acknowledgements

First of all I would like to thank Professor Eva Y. Andrei for her support and encouragement over the last months. She has read this thesis about 20 times and helped me to write it in a concise and correct fashion. I am grateful for all the discussions, comments and advises which you have had.

Special thanks go to Alem-Mar Goncalves and Ivan Skachko for their help with the lab routine, with all the difficulties I have had in making devices, learning how to use the machines in the lab, building the experimental set up and, of c(o)urse, good old Labview. Everything I know about Raman spectroscopy I have learned from Alem - And I will miss the discussions just about everything with Ivan. Thank you. I also want to thank Professor Phil Batson for his help with the TEM and the time he spent with me. I have learned a lot about electron microscopy from you. Then there is Justin, Adina, Yuanjun (my fellow desk neighbor) and Guohong. Thanks for the great time. Justin as my successor will continue the research presented here. I hope he will not find too many misinterpretations or errors in my work but I hope he can find them all!

The cooperation of the University of Würzburg and Rutgers is kept alive by Professor Fakher Assaad and Professor Ted Williams. Thank you for the opportunity to study at Rutgers. I have had a great time here. I want to thank the DAAD and the Elitenetzwerk Bayern for their financial support.

Dedication

"To Life, the Universe and Everything."

Table of Contents

List of Tables

List of Figures

Chapter 1

Introduction

Genetic information determines the structure of every organism. The information is *genetic* since it is inherited from one generation to the next. The total set of genetic information is called the *genome*. The process of reading out the genetic information is called *sequencing*. In biological systems the genetic information is stored in a molecule called deoxyribonucleic acid (DNA). DNA is a macromolecule built from four different monomers, the so called *nucleotides*. The sequence of the nucleotides is called the *DNA sequence*. The specific sequence of the DNA molecule is different for each organism. Due to advances in sequencing technology, it is possible to sequence entire genomes on reasonable timescales, however just about a few genomes are known entirely because the process is still quite slow. The ability to sequence a genome cheaply and efficiently will advance medicine as to diagnosis and appropriate treatment of diseases and the development of pharmaceuticals. Personal genomics promises a fast and reliable diagnosis of hereditary diseases and their treatment. Cheap and simple to use lab-on-a-chip devices for DNA sequencing have the potential to revolutionize many aspects of science from medicine to forensics. However these steps require more advanced techniques than currently available.

Many universities and companies have an interest in sequencing technologies. A recently published prize, the *Archon X prize* is a $10 million prize for the first team to successfully sequence a human genome for less then $1000 [31]. In the year 2004 the company *454 Life Sciences* developed a machine, using for the first time a massively parallelized pyrosequencing technology which is capable of sequencing 500 million base pairs in roughly 10h [124]. This is the fastest and most sophisticated apparatus for DNA sequencing so far. Roche Diagnostics purchased the company in 2007 for $154.9

million.

Single molecule DNA sensing devices promise cheap and fast sequencing. First attempts, so far unsuccessful in respect to single base resolution, involve nanopore sequencing. The first company to license a nanopore product is *Agilent Laboratories* in a cooperation with the Harvard university in the year 2001 [1]. However sequencing with molecular resolution is so far out of reach for nanopore machines. Nevertheless they have proven the ability to detect DNA and to distinguish between different DNAs.

The goal of this work is the construction of a a new type of sequencing device. We propose to use the measurement of a tunneling current across a trapped DNA strain with the idea to distinguish between the nucleobases from the difference in size and HOMO/LUMO levels. To reach the necessary spatial resolution we will use graphene as a tunneling electrode. This approach is similar to techniques proposed for nanopore research where platinum electrodes have been successfully embedded into the walls of a nanopore [42]. However we will use graphene tips embedded in a nano channel device. Since graphene imaging with a TEM is difficult on an amorphous substrate we will not do the nanofabrication of the tips with a TEM but using a new approach: we will produce graphene tips by burning graphene strips. The nanochannel, the contacts and the graphene strips are manufactured with e-beam lithography. The graphene used in this thesis is made by chemical vapor deposition (CVD) which is a large scale production method of high quality graphene [98].

First, we will give a broad introduction in the first chapter *"fundamentals"*. There we will outline the idea of a nanochannel sequencing device. The chapter *"theory"* deals with graphene, the theory of tunneling, electro-chemistry and the behavior of DNA in a nanochannel. Is covers more information than what we need - however it can be considered to be a review of the topic for a physicist. The chapter *"experiment"* shows our results so far. We show the fabrication of tip-like structures in graphene and tunneling curves through various materials. We can show evidence for molecule detection with a graphene device (in our case Rhodamine B). We show that Simmon's model

[1] "Agilent Laboratories, Harvard University Collaborate On Development of Breakthrough Technology for the Analysis of Nucleic Acids". Business Wire. 2001-05-21.

for tunneling is appropriate for highly doped graphene. We will measure the barrier height of different solvents in respect to graphene. The chapter *"measurement setup"* describes the laboratory setup for measurements and for the tip fabrication. In the chapter *"methods"* we describe the device fabrication in detail.

Chapter 2

Fundamentals

2.1 A short history of DNA

Deoxyribonucleic acid (DNA) is a molecule which can be found in every living organism known so far. It contains the genetic information which is the structure of all proteins that are produced by an organism and regions serving regulatory functions as well. Aside from water, minerals and small molecules, proteins are the main component of life. Some of them which are called enzymes, control chemical reactions; others, called the structure proteins are the framework of the cells. These two examples are covering a small fraction of all proteins families. In some sense proteins can be seen as the bricks of our bodies. DNA is mostly confined to the center of a cell, the nucleus. There it is transcribed to another macromolecule, the ribonucleic acid (RNA), which leaves the nucleus. Cell organelles called ribosomes then translate the RNA to a sequence of amino acids, a so called protein.

DNA as a substance was isolated in 1869 by the swiss physician Friedrich Miescher. He used leukocytes, the white blood cells, extracted from pus of surgical bandages [15]. Its composition from phosphoric acid, a sugar and four different molecules, called *nucleobases* has first been described in 1919 [60]. The role of DNA as the carrier of genetic information, the information which is inherited from one generation to the next, was identified in the 1940ies and 1950ies [4] [37]. The famous double helical structure was demonstrated by Watson and Crick in the year 1953 [131]. They were honored with the Nobel Prize in medicine in 1962. The analysis of the genetic code and an understanding how DNA is translated into an amino acid sequence took more time. First experiments in the early 1960ies showed that a triplet of bases encodes an amino acid [14] [86]. Marshall Nirenberg and Heinrich Matthaei managed to decode the first triplet, they

showed that poly-U encodes poly-phenylalanine [85]. Finally they deciphered 54 out of the total $4^3 = 64$ triplets. Har Gobind Khorana completed their work. In 1965 Robert Holley managed to decipher how ribosomes synthesize proteins from a RNA molecule blueprint [39]. In 1968 Khorana, Holley and Nirenberg were honored with the Nobel Price in medicine for their work on DNA encoding.

DNA itself is a macromolecule that consists of two complementary polymers which are bound by hydrogen bonds. The diameter of the so called double stranded DNA is roughly 1nm, one nucleotide unit measures 0.33nm in height. The two strains are wound around each other and appear in a double-helical shape. A single DNA strain itself consists of a backbone of sugar (deoxyribose) and phosphate. Each sugar is additionally bound to one of four nucleobases: Adenine (A), Guanine (G), Cytosine (C) and Thymine (T).

Fig. 2.1 shows the chemical structure of the nucleobases. The five[1] bases belong, due to differences in the chemical structure, to two different classes of molecules: Adenine and Guanine are purine bases; Thymine, Cytosine (and Uracil) are pyrimidine bases. Fig. 2.1a shows the backbone of a DNA strain. Phosphate and deoxyribose alternate and a nucleobase is connected to every deoxyribose molecule. The nucleobases are shown in fig. 2.1b. Due to the asymmetry in the sugar molecule, DNA has a certain directionality. The ends are called 5' (five prime) and 3' (three prime), related to the carbon atom in the deoxyribose molecule. The reason that two DNA strains bind together are hydrogen bonds between the nucleobases on one side and a stacking of the hydrophobic π-bonds of the nucleobases on the other. Adenine links with Thymine and Cytosine with Guanine via hydrogen bonds. Therefore the bases appear as pairs. Both DNA strains carry a different sequence of nucleic acids. Genetic information is in general stored on both sides of the DNA molecule. The two DNA strains are referred to as *Template Strain* and *Coding Strain*.

If DNA is exposed to high temperatures, the bonds that hold both strains together weaken. Ultimately the link will break and double-stranded DNA will become two molecules of single stranded DNA (ss-DNA). The DNA denaturation is called melting.

[1] Five bases if one takes Uracil into account which replaces Thymine in RNA.

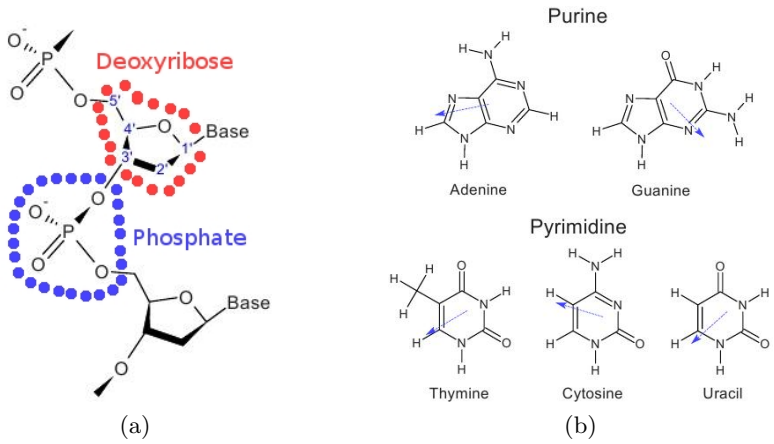

(a) (b)

Figure 2.1: The structure of the DNA molecule. **a**, The DNA backbone consists of phosphodiester bound deoxyribose molecules. They are referred to as phosphate (blue) and deoxyribose (red) group. The sequence of carbon atoms in the deoxyribose indicates a 3' and a 5' end. 5' to 3' and vice versa define a directionality in a DNA strain. **b**, Attached to the backbone are four nucleobases. The sequence of the nucleobases carries the genetic information. We show an image of the two Purine bases: Adenine and Guanine and the three Pyrimidine bases: Thymine, Cytosine and Uracil. The two images are copied and adapted from [137]. The arrows in the nucleobases indicate the direction of the dipole moment.

The melting temperature T_m depends on the nucleobase content of the DNA molecule, however at about $90°C$ all ds-DNA breaks to ss-DNA.

RNA is very similar to DNA since it is also a macromolecule with a backbone of sugar and phosphate, which is bound to four different nucleobases. However deoxyribose is replaced by the sugar ribose and the nucleobase thymine is replaced by Uracile (U). Besides RNA is single stranded. Uracile is also shown in fig. 2.1b. RNA is the carrier of genetic information from the nucleus to the ribosomes.

The human genome has a length of about 3 billion base pairs which are ordered in 23 chromosomes, structures that are build from ds-DNA molecules which wind around proteins called histones [13] [31]. Therefore each human cell contains 23 double stranded DNA molecules. The smallest genome of a living organism known so far has a length of 159662 base pairs. It belongs to a bacterium with the name Candidatus Carsonella ruddii [82]. A virus requires living cells to replicate, therefore it is not considered being a life form. Viruses have even shorter genetic codes. The shortest RNA sequence with the ability to reproduce itself has a length of 189 bases [45].

There are several types of DNA as to different configurations from different hydrogen bonds. However, one winding of the helical structure of the DNA realized in nature (so called B-DNA) consists of 10 base pairs at a length of $3.4nm$. Double stranded B-DNA (ds-DNA) has a diameter of $\approx 2.4nm$. DNA is negatively charged by the phosphate groups. 10 base pairs carry 20 negative charges, thus ds-DNA has a constant charge per length of $\rho = 0.942\frac{nC}{m}$[2]. That is the reason that DNA migrates in an electric field towards the positive pole. In its natural liquid environment DNA is accompanied by positively charged ions which are attracted by the negative charge. Common ions in biological systems are K^+, Na^+, Mg^{2+} and Ca^{2+}.

DNA decoding works in two steps, at first DNA is transcribed to RNA and then translated to a protein sequence. In the transcription DNA is read from 3' to 5' whereas RNA is created from 5' to 3'. The template DNA strain is used for transcription. Therefore the m-RNA sequence reads as the coding strain. A simple example will make it clear: The sequence of a DNA fragment which reads *3' ACCTAGGTACTA 5'* on the template strain is bound to a sequence of *5' TGGATCCATGAT 3'* on the coding strain. The m-RNA fragment associated with this piece of DNA is *3' UGGAUCCAUGAU 5'*. The next step is the m-RNA translation to a protein. Biology on earth uses a total set of 21 amino acids. Two nucleobases can make $4^2 = 16$ combinations. 3 nucleobases can have $4^3 = 64$ combinations. Therefore nature uses a triplet of nucleobases to encode the 21 amino acids and one stop signal. A nucleobase tiplet is also called a *codon* since it is the smallest unit of information. In the example given, UGG encodes Tryptophane, AUC encodes Isoleucine, CAU Histidine and GAU Aspartic Acid. Therefore the protein fragment encoded would be Tryptophane - Isoleucine - Histidine - Aspartic Acid.

2.2 Sequencing methods

The discovery of a technique to obtain the sequence of base pairs of a given DNA molecule was a giant leap for science. DNA sequencing is used in the identification of cancers, germs, bacteria and viruses. It is also used for the creation and analysis of

[2]The charge is $\rho = 10 \cdot (2\,bases) \cdot 1\frac{phosphate}{base} \cdot 1\frac{e}{phosphate} \cdot \frac{1}{3.4nm}$

genetically modified organisms, research on ancestry and heredity and bottom-up research in proteomics. Even entirely different scientific fields as paleontology, prehistory and archeology use structure analysis of DNA.

The first technique of sequencing DNA was introduced by Frederick Sanger in the year 1975 [105] and honored with the Nobel Prize in chemistry in 1980. He proposed a chain termination method [105] [106] which works as follows: DNA can be replicated by enzymes called polymerases. Those enzymes require base-sugar-phosphate monomeres, which are called nucleotides, from which a second strain of DNA is build along a yet existing ss-DNA molecule. Sanger added a small amount of a chemically altered nucleotide, which is marked radioactively and which stops the replication process at the position where it is built into the strain. He did so four times using just one chemically altered substance either for A, T, C, or G. In the end he obtained a mixture of DNA molecules of different length, all terminated with a marked nucleotide. By application of an electric field he separated the DNA molecules as a function of their length. So one can read the DNA sequence by reading the sequence of the markers.

Another technique introduced by Allan Maxam and Walter Gilbert uses a chemical breakdown of the DNA molecule [74]. They used a large amount of DNA and cut it chemically at A, C, T and G separately. They marked the cut region and obtained a similar mixture of DNA fragments that were again separated in an electric field.

Today a variant of Sanger's method is used. His technique has been used, in a massively parallelized fashion, to sequence the human genome. However chain termination techniques as Sanger's method have some disadvantages: One can only sequence small fragments of DNA and expensive chemicals are necessary.

A completely new approach was introduced by Kasianowicz et al. in 1996 [48]. A so called nanopore, a small hole, permeable just for a single DNA molecule, could be used as a probe on a molecular scale. Kasianowicz used a protein pore, the so called Hemolysin-α protein, embedded in a lipid membrane in a liquid environment. The measurable signal is the blocking of ionic current when DNA passes the pore. The technique promises that only a single molecule is necessary to obtain a sequence. Thus no expensive chemicals are needed for the sequencing process. Numerous experiments

with biological pores [1] [3] [9] [73] [77] [78], synthetic pores in bulk materials [7] [10] [12] [24] [36] [64] [114] [136] and graphene [28] [79] [107] have been performed since. However single base resolution could not be reached due to the high speed[3] of DNA of $40\frac{ns}{bp}$ at $\approx 100mV$ bias while passing a nanopore. Suggested possible solutions to overcome the problem are an increase in viscosity of the environment and/or a smaller applied voltage at the pore. Using an increased viscosity due to glycerol as an additive a translocation speed of $300\frac{ns}{bp}$ through the nanopore could be reached [25]. Typical tunnling currents of the order of 1pA can be measured with a sampling rate of 1kHz[4]. Therefore DNA has to slow down to about $1\frac{ms}{bp}$. The bias voltage can not be chosen arbitrarily small due to the increasing noise levels. However some principal problems still remain, such as Brownian motion of the DNA within the nanopore and a cone shaped ion flow through the nanopore which is not localized enough to resolve a single nucleotide [7]. Even though nanopore technologies have serious difficulties as to sequencing they have a variety of applications [128] [129] [130].

In recent years the idea came up to use tunneling as a sequencing tool. This is in particular related to nanopore research since a tunnel probe can be built into the walls of a nanopore to measure tunneling currents while the same time measuring the blocking of longitudinal ionic current. A nanopore experiment with an embedded platinum tunneling electrode has recently been performed and shows promising results as to tunneling measurements [42]. One principal problem for metal electrodes in general remains; metal structures are bulky. It is extremely difficult to measure a single molecule passing through a gap in a bulk conductor. Graphene is a natural choice to overcome this problem.

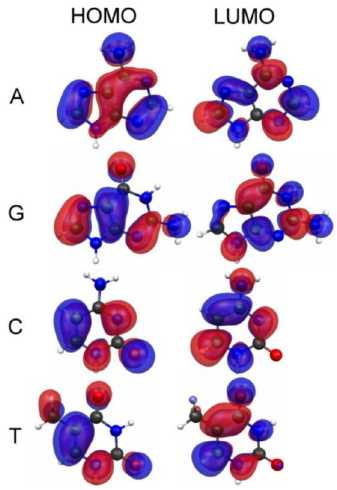

Figure 2.2: Highest occupied and lowest unoccupied molecular orbitals of the four DNA nucleobases. Colors indicate the relative phase of the orbitals. Graphic copied and adapted from [137].

2.3 Tunneling measurements as sequencing tool

The idea to sequence DNA by means of tunneling came up with the first STMs since a measurement of a tunnel current can distinguish between the different HOMO/LUMO-Levels and the relative size of the nucleobases. HOMO stands for the "Highest occupied molecular orbital" and LUMO for the "Lowest unoccupied molecular orbital". The HOMOs and LUMOs for the four DNA nucleobases are shown in fig. 2.2. Experiments using a STM and DNA on gold seem promising [103] but it has so far fallen short of delivering a simple sequencing technology.

Scanning tunneling spectroscopy became the standard tool of analyzing single molecule thick layers of material since its proof of principle in 1997 [17]. It is used for the study of orbitals, e.g. [40] and also for objects like molecular wires, e.g. [121]. The problem that a bulk electrode from gold is too large to contact a single base in a DNA molecule has been addressed by chemically modified bulk material electrodes [35]. Models predict that by using single atomic layer electrode materials, namely graphene and allowing a DNA molecule to go through the tunneling gap the resolution should exceed the resolution of bulk electrodes by far [84] [94] [95] [135].

---

[3] Actually $\frac{ns}{bp}$ corresponds to the inverse of a speed.

[4] For example with the Keithley 427 Current Amplifier

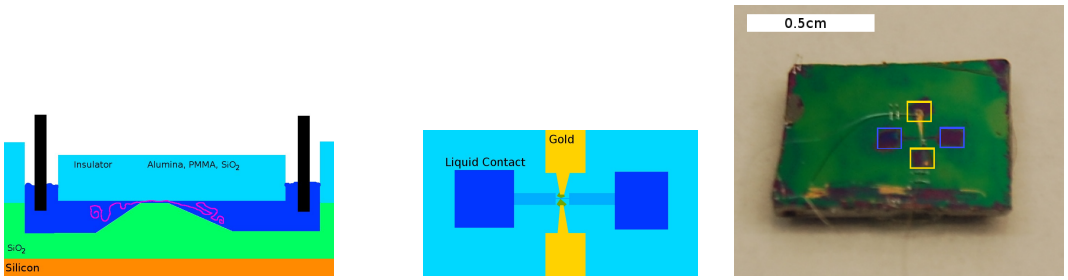

(a) (b) (c)

Figure 2.3: The nanochannel device realized in this thesis is shown. **a**, DNA (pink) is confined in a nanochannel. It is placed there by electrodes (black) which are used to apply an ionic current through the liquid (dark blue) to move the electrically charged DNA molecule. Once located in the nanochannel, tunneling current across the molecule can be measured from graphene electrodes. **b**, The nanochannel device in top view. The longitudinal nanochannel (dark blue) is contacted with tho graphene tunneling probes (green) which are contacted with Au/Ti leads (yellow). **c**, An image of a fully fabricated nanochannel device is shown. The blue boxes indicate the access ports for the nanochannel; the yellow boxes show where the tunneling probe is contacted. The wirebonding wire to contact the gold leads in the yellow boxes can also be seen.

The object of this thesis is to develop a method of forming tunneling junctions in graphene. Subsequently we want to use graphene tunneling junctions to distinguish between molecules. We will embed graphene tunneling electrodes in a nanochannel to show the feasibility of the nanochannel sequencing idea. The chip design proposed in this thesis is shown in fig. 2.3. A carrier chip covered with a layer of silicon oxide and two graphene tunneling probes embedded transversely in a nanochannel is used to measure a tunnel current through molecules within the channel. Electrically charged molecules as DNA can migrate along the nanochannel if an electric field is applied. Tunneling probes in nanochannels have previously been realized and have also been used for probing DNA [72] [66], however the electrode material was gold and a single nucleobase resolution could not be achieved.

2.4 DNA and nanochannels - an overview

Earlier work on DNA within a Poly(methyl-methacrylate) (PMMA) nanochannel has shown that DNA can be stretched out and that PMMA nanochannels can be made with e-beam lithography [26] [99] [119] [120]. We will therefore use a similar PMMA nanochannel to control the movement of the DNA molecule. The nanochannels used in

this thesis will be fabricated with e-beam lithography and wet etching of a sacrificial gold layer, similar to a technique proposed by Eijkel et al. [19] [112]. We use PMMA as channel material as well as sputtered Al_2O_3. PMMA has the advantage that it is easy to work with; Alumina is more rigid and makes nanochannel devices reusable. Previous measurements of the mobility of DNA in narrow nanochannels have shown that the highest mobility for λ-DNA in fused silica nanoslits is achieved with electrical fields of $20kV/m$ (The authors explain the remarkable observation of a smaller mobility at higher fields with a mechanism of friction between the molecules and the substrates) [104]. We want the DNA molecule to migrate through the nanochannel slowly to have a well measurable tunneling current corresponding to a single base. We will therefore construct a device with a relatively long nanochannel. A more quantitative train of thought is presented in chapter 3.

Chapter 3

Theory

3.1 Graphene

Graphene as an actual material that can be isolated and investigated in the laboratory is less than a decade old. Andre Geim and Kostya Novoselov described the isolation of crystalline carbon monolayers by exfoliation from graphite bulk material on silicon oxide for the first time in 2004 [89]. This discovery was honored with the Nobel Prize in physics in the year 2010. It is not only a material of unique thinness, it is also a material of unique electronical properties. The band structure of a hexagonal lattice is conical. It consists of two electron-hole symmetric cones which are related to each other by time reversal symmetry. Therefore the quasi particles in graphene emulate ultra-relativistic particles with $c = v_F$ [125]. A linear dispersion relation $E = v_k|k|$ gives rise to a linear density of states (DOS) $D(E)$:

$$D(E) = \frac{dN}{dE} = \frac{dN}{d^n k}\frac{d^n k}{dE} = \left(\frac{L}{2\pi}\right)^2 \cdot 2\pi k \cdot \left(\frac{dE}{dk}\right)^{-1} \propto k \propto E \tag{3.1}$$

The Fermi Level of graphene is located at the so called *Dirac Point*, the point where valence and conduction bands touch and where the DOS is zero. If the Fermi energy is shifted, by doping or by gating, the resistivity of graphene changes quite dramatically. However graphene is in general a good conductor.

Kinks in the DOS of single layer graphene occur at $\approx \pm 2eV$ around the Dirac Point due to saddle points in the dispersion relation. A detailed study of the DOS of graphene can be found in [101]. The Van Hove singularities of graphene are studied in multilayer systems [62]. If tunneling measurements in the regime of a few volts are possible, one should be able to see the influence of the Van Hove singularities in the DOS to the tunneling current. Tunneling characteristics of graphene as a material are studied in

detail elsewhere [61] [63] [70].

Doped graphene can be gated to shift the Fermi energy back to the Dirac point.

The idea of gating is the introduction of a charge Q per area A into graphene. An applied voltage V_g between graphene and a conducting material next to graphene does the trick. The charge per area is simply

$$\frac{Q}{A} = \frac{C}{A} \cdot V_g \tag{3.2}$$

where C is the capacitance between graphene and the gate. The carrier density n is the charge density divided by the elementary charge, therefore

$$n = \frac{1}{e}\frac{C}{A} \cdot V_g \tag{3.3}$$

A positive gate voltage corresponds to electron doping while a negative gate voltage gives hole doping. The carrier density is related to the Fermi momentum k_F by

$$\frac{L^2}{(2\pi)^2}\pi k_F^2 = N \tag{3.4}$$

in a square with a side length L and a total number of particles N so that

$$|k_F| = \sqrt{4\pi n} = \sqrt{4\pi\frac{C}{eA}} \cdot \sqrt{|V_g|} \tag{3.5}$$

With the known linear dispersion relation the Fermi energy E_F as a function of V_g reads

$$E_F \propto \sqrt{V_g} \tag{3.6}$$

3.2 Tunneling measurements

3.2.1 Introduction

The principal setup for tunneling measurements is shown in fig. 3.1. Firstly we consider tunneling from two conductors through vacuum. The tunneling current depends on the density of states of both tips[1]

$$I = \int_{-\infty}^{\infty} T(\epsilon)\rho_1(\epsilon)\rho_2(\epsilon + eU)\left(f_1(\epsilon) - f_2(\epsilon + eU)\right) d\epsilon \tag{3.7}$$

[1]Can be found as eqn. 1.43 in [133].

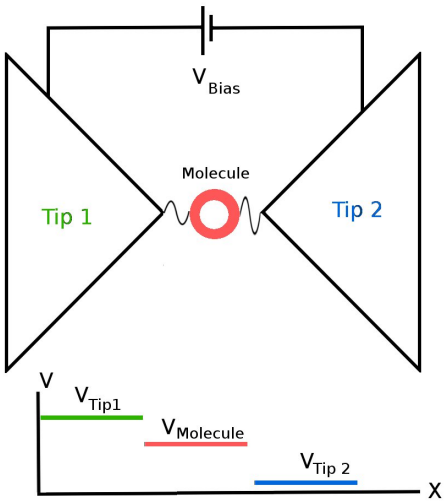

Figure 3.1: Tunneling probe for measuring a molecules. Two graphene tips contact a molecule (red ring) with a bias voltage V_{bias}.

and $T(\epsilon)$ which is the transmission probability. The transmission probability depends on the distance of the tips or if there is a molecule between the tips. $f_{1,2}(E) = \frac{1}{e^{\frac{E-E_F}{k_B T}}+1}$ is the Fermi-Dirac distribution at a temperature T for the Fermi energy E_F. $\rho_{1,2}$ is the DOS of the two tips and U is the voltage between the two tips; $e = 1.602 \cdot 10^{-19} C$ is the elementary charge.

Due to different scales of Fermi energy (few eV) and room temperature $k_B T \approx 30meV$ so that $E_F >> k_B T$ the equation above can be approximated as follows:

$$I \propto \int_0^{eU} T(\epsilon)\rho_1(\epsilon)\rho_2(\epsilon + eU)d\epsilon \tag{3.8}$$

The transmission coefficient T takes the distance into account. If the tips are far apart, T is very small and there is just a vacuum tunneling. If a molecular orbital lies in between the tips, the electrons can tunnel into the molecule and from the molecule to the next tip. This case is shown in fig. 3.1 where we referred to the wave function of the tunneling electron as a wiggly line. Important for tunneling through molecules are HOMO and LUMO. They will show if tunneling measurements are performed. Tunneling to the molecule and from there to the second tip is in general possible if the tunneling electron has the same energy as the sharp molecular energy values ϵ_n. We

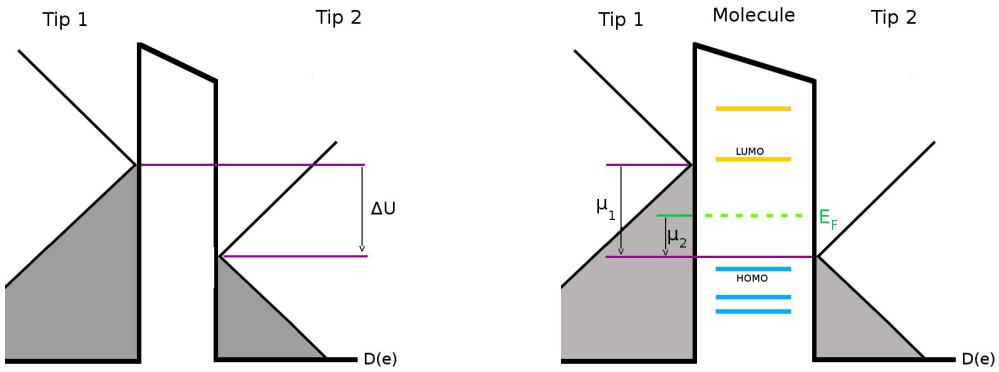

Figure 3.2: Tunneling between graphene tips with and without a molecule in between. **a**, Tunneling without a molecule between the tips. The occupied states are gray; both Fermi energies lie in the Dirac point. An applied voltage of ΔU shifts both relatively and a few electrons can tunnel across the gap. **b**, Tunneling with a molecule between the tips. The molecular orbitals align with the Fermi energy of the graphene tips. Occupied molecular orbitals are indicated as blue, unoccupied molecular orbitals are indicated as yellow. This particular molecule will not enhance transport across the tunneling gap because there are no molecular energy states between the respective chemical potentials of the graphene tips. If the bias voltage is increased a little more, molecular states will increase the transport across the junction.

can therefore say:

$$T(\epsilon) = T_{vac} + \sum_{i=0}^{N} \delta(\epsilon - \epsilon_i) C_i \tag{3.9}$$

with a vacuum transmission probability T_{vac} and a higher transmission probability for the molecular states, each weighted due to differences in size with a constant C_i. Starting from this simple model we expect to see peaks in the $\frac{dU}{dI}$ curve as long as the the DOS of the tips is more or less constant[2]. For tunneling through a molecule the absolute position of the energy levels of the molecule is important. If there is no orbital state between the energy levels of the tips E_1 and $E_1 + eU$, the conductivity through the molecule is very small. A key question is where the molecular energy states are located in reference to the electronic bands. It is difficult to apply the concept of a Fermi energy to a single molecule, although it is done [54] [76]. We have therefore indicated a Fermi energy in the molecule in fig. 3.2b. It is often more instructive to think about

[2]This description for the transmission probability is very crude. We will elaborate it in the next section and Appendix **A.** .

an alignment of the molecule energy states to the energy states of the contacts. It is in general a difficult topic and requires a lot of theoretical effort, mostly via DFT [76] [113]. There is no simple concept on how molecules behave in the vicinity of tunneling probes. Graphene as a transparent material is interesting for solar cell applications. In dye-sensitized solar cells the alignment of the dye's HOMO/LUMO in reference to the electrode material is important for the efficiency. However the absence of a general and simple method to calculate the alignment of the energy levels is just as problematic [126].

Gating of a molecule between two contacts is possible albeit difficult. The electric field related to a distant gate electrode is not strong enough to influence the Fermi Level of a molecule. A common technique for gating molecules is the electrochemical modification of the molecule itself. A Redox reaction can introduce charge into the molecule which will change the molecular energy levels [33]. Fig. 3.1 also shows the potential profile across the tunneling gap. $V_{molecule}$ strongly depends on the position of the molecule within the gap[3]. There are many reviews on tunneling though molecules and the electrical properties of single molecules in general [11] [32] [76] [108] [118]. We also present information from several theoretical papers [16] [18] [43] [52] [87] [88] [102].

3.2.2 Tunneling through liquids

Simmons' model for tunneling between two metallic electrodes through an insulating material is successfully used for tunneling through liquids [110]. It is applied for a homogeneous energy barrier between two metal contacts. This is a good approximation for highly doped or gated graphene with air or water between the contacts. Voltage-Current data can be fit to the function:

$$I = \frac{Aq}{2\pi h d^2}\left(\left(q\phi_0 - \frac{qV}{2}\right)e^{-\sqrt{C\cdot\left(q\phi_0 - \frac{qV}{2}\right)}} - \left(q\phi_0 + \frac{qV}{2}\right)e^{-\sqrt{C\cdot\left(q\phi_0 + \frac{qV}{2}\right)}}\right) \quad (3.10)$$

where $C = \frac{32\pi^2 d^2 m_e}{h^2}$, q and m_e are the charge and the mass of the electron, A is the area cross-section of the junction, d is the distance, ϕ_0 is the barrier height in [eV] and

[3] In general a not-centrally located molecule will give rise to asymmetries in the tunneling spectra. More to the influence of asymmetry can be found in [54].

Substance	ϕ_0	$I(U = 0.3V)$
Water	0.93eV	40nA
Isopropanole	1.68eV	0.7nA
1-Butanole	2.63eV	14pA
Benzene	3.85eV	0.7pA
Carbontetrachloride	4.16eV	90fA

Table 3.1: Shown is an overview of tunneling barrier height ϕ_0 and typical tunneling current for different materials from experimental data and fits to Simmons' model. The tunneling current has been measured with a bias voltage of $0.3V$. Prokopuk et al. build nanostructures from two gold leads on the bottom and the top side of a nanochannel [96]. The distance between the gold electrodes (the tunneling gap) has been adjusted to $\approx 4nm$. The cross-section of the area at which tunneling can take place is $1600nm^2$. Therefore a fit with Simmons' model is limited to one free parameter ϕ_0 and the measurement of the barrier height is relatively precise.

h is Planck's constant. V is in units of volts and I is in units of amps. Simmons' model starts from the WKB approximation for tunneling and further simplifies the result by the assumption of a mean barrier height ϕ_0 of the potential through which the electrons have to tunnel. The two terms are a result of tunneling of one electrode to the other and vice versa.

Tab. 3.1 shows a few values for the barrier height of different liquids in reference to gold. It seems to be a good rule of thumb that hydrogen bonding solvents have smaller barrier heights than polar solvents and polar solvents have smaller barrier heights than apolar solvents. Therefore we should prefer apolar solvents for our measurements. However, since DNA is a polar molecule which has a high solubility in water it is reasonable to measure tunneling currents in polar environment as water.

3.2.3 Tunneling through DNA and effects of noise

A model Hamiltonian can be constructed to couple two tunneling electrodes to a molecule's HOMO or LUMO which again couples to a bosonic noise source. The Hamiltonian is originally used to describe resonant tunneling junctions with phononic noise.[43] [52]

$$H = E_0 d^\dagger d + H_{de} + H_e + d^\dagger d \sum_k g_k \left(b_k^\dagger + b_k \right) + \sum_k \omega_k b_k^\dagger b \tag{3.11}$$

Variable	Value
E_0	1eV
γ_m	6.8×10^{-4} eV
σ_γ	0.45

Table 3.2: Typical parameters for the electrode molecule coupling as described in the model to fit signals as in fig. 3.3. The values are copied from [52].

$E_0 d^\dagger d$ accounts for the electrons within the HOMO/LUMO, H_{de} is the DNA-electrode interaction, H_e the electrodes' Hamiltonian itself. $\sum_k \omega_k b_k^\dagger b$ represents a bosonic environment which interacts with the electrons in the molecule via $d^\dagger d \sum_k g_k \left(b_k^\dagger + b_k\right)$. This Hamiltonian allows to calculate a Green's function and from the Green's function the conductivity of the tunneling junction. The calculation is given in more detail in appendix A. The current across the junctions takes the form

$$I(\eta) = \frac{2e^2 V}{h} \left(\frac{\gamma^2}{E_0^2 + (\gamma + \eta)^2} + \frac{\eta\gamma}{E_0^2 + (\gamma + \eta)^2} \right) \tag{3.12}$$

$\eta = \frac{\hbar}{\tau}$ corresponds to a timescale τ of the bosonic noise. It produces Lorentz broadened resonance peaks and accounts for a small shift. Noise in coupling γ with a certain width σ_γ which arises from different molecule orientations will result in a logarithmic broadening of the peaks[4]. This effect can be seen in the broadening of the peaks in fig. 3.3. A detailed description of this model can be found in the paper of M. Krems et al. [52].

To reach the goal of sequencing DNA the regions of current measurements have to be well separated. Typical values for the distribution of molecule-electrode couplings are given in tab. 3.2. Those values have been calculated from molecular dynamic simulations [52]. Fig. 3.3 shows the distribution of signals modeled ab initio.

We learn from the calculation above that a specific molecule at a constant bias voltage will produce different currents. Therefore the current through the junction for two different bases can be the identical. This is a principal problem that we can not overcome by better measurements. However it can be solved by statistics: If a specific spot on the DNA molecule is measured very often so that the current distribution as in fig. 3.3 is obtained, the nucleobase can clearly be identified. In general statistics will

[4] As in eqn. A.12 in appendix A.

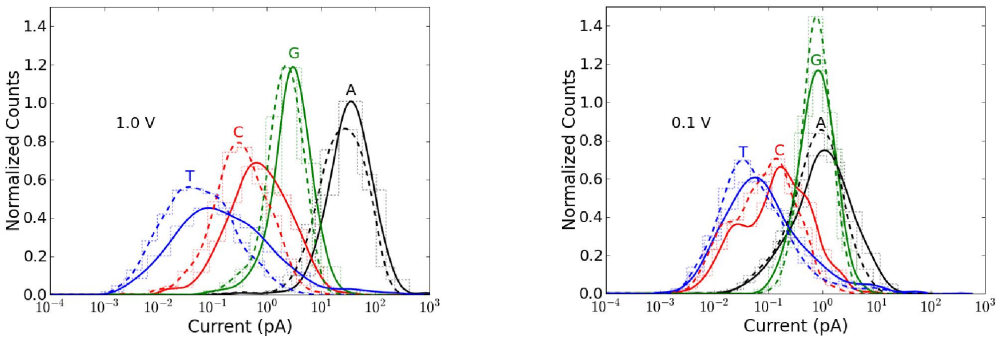

(a) (b)

Figure 3.3: Tunneling signals calculated from molecular dynamics simulations for the different DNA bases migrating through a silicon nitride nanopore in 1M potassium chloride solution with a minimal diameter of 1.4nm and bulk metal electrodes. Solid lines correspond to $\eta = 0$, dashed lines correspond to a timescale of $\tau = 10^{-15}s$. Both plots are from [52]. **a**, The signal range is shown for a bias voltage of 1V between the embedded electrodes. **b**, The same plot as before but with a bias voltage of 0.1V.

be an important aspect of successful sequencing [95]. Besides statistics are extremely helpful for low level measurements considering currents through the tunneling junction as small as a few fA.

3.3 On DNA in the system

3.3.1 Charges in a liquid environment

Since DNA is electrically charged, it is necessary to understand how charges behave in an environment that contains ions.

The electrical potential is in general associated with a charge density ρ by the Poisson-equation

$$\Delta\phi = -\frac{1}{\epsilon}\rho \tag{3.13}$$

with a known permittivity $\epsilon = \epsilon_r\epsilon_0$. The charge density in a liquid is expressed by the ion concentration c. Those ions move in the potential ϕ, described by the Boltzmann-equation:

$$\rho = -c\left(qe^{\frac{\phi q}{k_BT}} - qe^{-\frac{\phi q}{k_BT}}\right) \tag{3.14}$$

so that

$$\Delta\phi = \frac{1}{\epsilon} c \left(q e^{\frac{\phi q}{k_B T}} - q e^{-\frac{\phi q}{k_B T}} \right) \tag{3.15}$$

and with $\bar{\phi} = \frac{\phi q}{k_B T}$

$$\Delta\bar{\phi} = c \frac{q^2}{k_B T \epsilon} \left(e^{\bar{\phi}} - e^{-\bar{\phi}} \right) \tag{3.16}$$

This equation is often written as

$$\Delta\bar{\phi} = \lambda_D^{-2} \sinh(\bar{\phi}) \tag{3.17}$$

which is the Poisson-Boltzmann-Equation. $\lambda_D = \sqrt{\frac{1}{2} c \frac{q^2}{k_B T \epsilon}}$ is the Debye length, a characteristic length scale where charge is screened in an electrolyte[5]. Typical values for room temperature and 0.1 molar salt solutions are $\lambda_D \approx 1nm$ [6]. For some cases this differential equation can be solved analytically. One case is the homogeneously charged surface with surface charge density σ_q where the potential takes the form

$$\phi(x) = -\frac{\sigma_d \lambda_D}{\epsilon} e^{-\frac{x}{\lambda_D}}. \tag{3.18}$$

An electrode exposed to an electrolyte as water will have a potential as given above (as long as the voltage is small enough to prevent electrochemical processes to take place). DNA is electrically charged by the phosphate groups in the backbone. It will therefore attract a number of counterions from the liquid to screen the charge. However this process may not be imagined as a well defined movement of ions towards the DNA strain. It is rather a random walk in three dimensions until an ion randomly finds the DNA.

3.3.2 DNA in water

The next problem is describing the dynamics of a DNA molecule in water. A very simple approach is as follows: DNA can be described by a chain of N monomers of

[5] Far away from the charge where the potential is small, $\sinh\bar{\phi} \approx \bar{\phi}$ and therefore $\bar{\phi} \propto \exp(-\lambda_d z)$.

[6] Chapter 7 in [83] or [5].

length l, each independently random walking. The total length of the molecule is Nl. The vector from the first monomer to the last monomer is

$$\vec{x}_N = \sum_{i=1}^{N} l\vec{s}_i \tag{3.19}$$

where $\vec{s}_i$ is the direction vector between the monomer i and $i+1$ and l is the length between two monomers. Since the motion of the monomers is random

$$\langle \vec{s}_i \rangle = 0 = \langle \vec{x}_N \rangle \tag{3.20}$$

A single monomer is stiff, so that $\langle \vec{s}_i^2 \rangle = 1$. Also the motion of two monomers is independent $\langle \vec{s}_i \cdot \vec{s}_j \rangle = \langle \vec{s}_i \rangle \cdot \langle \vec{s}_j \rangle = 0$ Therefore

$$\langle \vec{x}_N^2 \rangle = Nl^2 = Ll \tag{3.21}$$

A better model is a worm-like chain, where the monomers cannot move completely free. In this model the correlation between two monomers is

$$\langle \vec{s}_m \vec{s}_n \rangle = e^{-l\frac{|n-m|}{\xi}} \tag{3.22}$$

with the persistence length ξ. $\langle \vec{x}_N^2 \rangle$ in this model reads

$$\langle \vec{x}_N^2 \rangle = \sum_{m,n} l^2 e^{-l\frac{|n-m|}{\xi}} \approx 2\xi l N = 2\xi L \tag{3.23}$$

The latter model is better suited for DNA, which is a quite stiff polymer. The persistence length is $\xi \approx 50nm$. λ-DNA has a length of 48490 bp which corresponds to $0.33\frac{nm}{bp} \cdot 48000bp = 15\mu m$. So the typical size of a DNA blob in water is $\sqrt{\langle \vec{x}_N^2 \rangle} \approx 1.2\mu m$

3.3.3 DNA in a nanochannel

The Navier-Stokes-Equation describes the behavior of liquids. It reads

$$\rho\left(\frac{\partial v}{\partial t} + v \cdot \nabla v\right) = -\nabla p + \eta \Delta v + f \tag{3.24}$$

with the density of the liquid ρ, the velocity v, the pressure p, the viscosity η ($\eta \approx 10^{-3} Pa \cdot s$ for water at room temperature) and an external force density f. For the

steady state case and an incompressible liquid with no pressure gradient the equation simplifies to:

$$0 = \eta \Delta v + f \tag{3.25}$$

This equation can be used to estimate the necessary force to drag a DNA filament through a nanochannel: Across the nanochannel there is no pressure gradient and the DNA molecule is dragged by an electric field. As a simplification of the problem we can consider the DNA molecule to migrate through a cylindrical nanochannel with a radius d and a length L. DNA itself can be considered as a cylinder moving in the center of the pore with a radius a and a migration velocity v_{DNA}. The Laplace operator in cylindrical coordinates reads $\Delta g(r) = \frac{1}{r}\frac{\partial}{\partial r}\left(r\frac{\partial g}{\partial r}\right)$. The equation above can be solved for the force density of a moving cylinder, which is zero everywhere except for a small region near the surface $f = \frac{F_0}{2\pi L a}\delta(r-a)$ by

$$v = \frac{F_0}{2\pi L \eta} \cdot \log\left(\frac{d}{r}\right) \tag{3.26}$$

with the boundary conditions $v(a) = v_{DNA}$ and $v(d) = 0$. Therefore

$$v_{DNA} = \frac{F_0}{2\pi L \eta} \cdot \log\left(\frac{d}{a}\right) \tag{3.27}$$

The force per length is related to the electric field and the charge per length $\rho = 5.88\frac{e}{nm}$.

$$\frac{F_0}{L} = E \cdot \rho = \frac{U}{L} \cdot \rho \tag{3.28}$$

where U is the voltage drop and L is the length of the nanochannel.

$$v_{DNA} = \frac{U}{L}\frac{\rho}{2\pi\eta} \cdot \log\left(\frac{d}{a}\right) \tag{3.29}$$

For a typical nanochannel[7] with $d \approx 3nm$, $a \approx 1nm$ and $L \approx 1\mu m$

$$v_{DNA} \approx 70\frac{\mu m}{sV} \cdot U \approx 0.2\frac{bp}{ns \cdot V} \cdot U \tag{3.30}$$

We can control the mobility of DNA not only by the voltage but also by the geometry of the channel.

[7]The nanochannel we consider here is more like a nanopore. Therefore the translocation speed is close to 1-10$\frac{bp}{ns}$ at 1V bias which is a typical value for nanopores.

3.3.4 Some measurements on drag forces

There are no studies on how much force is necessary to drag a DNA molecule through a nanochannel. Studies with nanopores however indicate that more force is required than what we estimated with the calculation above. Keyser et al. find for a solid state nanopore with a diameter of $\approx 10nm$ and a length of $60nm$ a force acting on the DNA molecule of $0.25\frac{pN}{mV}$ for λ-DNA which indicates a smaller effective charge [49]. A likely reason is the shielding of the charge in a liquid environment. Meller et al. directly measure the translocation speed - voltage curve for biological nanopores. They report a nonlinear behavior of the mobility, however a linear fit for their data is still acceptable [77]. It gives a mobility of $\approx 1\frac{mm}{sV}$. The biological pore they use, an α-Haemolysin Complex, has a diameter of $0.9nm$ and a length of $5nm$. However biological pores are not very reliable as a point of reference due to DNA protein interactions. Solid state pores as described by Fologea et al. do a better job. They report a translocation speed of 3 $\frac{bp}{\mu s}$ at a bias voltage of $20mV$, a nanopore diameter of $\approx 6nm$ and a length of $280nm$ [25]. To slow the DNA down (the mobility of the DNA molecule goes as L^{-1} of a nanopore/nanochannel as we calculated previously) they make nanopores as long as possible. They push the limits of TEM fabricated nanopores with membranes as thick as $280nm$.

Here we find a huge advantage for nanochannel devices since it is not a problem to produce nanochannels of arbitrary length.

3.4 Electro-chemistry of the nanochannel devices

Ag/AgCl electrodes, fabricated from a piece of silver wire[8] are used as a low resistivity interface between the regime of electronic conductance in the wires and ionic conductance in the liquid, here water. A drawing of the system is given in fig. 3.4. The silver electrodes are covered with a thin and porous layer of silver chloride, which allows the electrolyte to be in close contact with both materials. The cathode reaction is:

$$Ag^+ + e^- \rightarrow Ag$$

[8]The Method is described in the section "Methods".

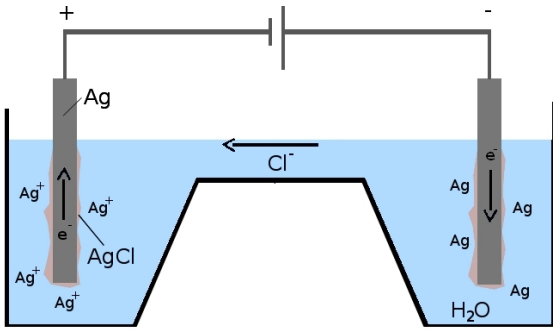

Figure 3.4: A diagram of the Ag/AgCl Interface of the nanochannel device.

and the reaction at the anode vice versa

$$Ag \rightarrow Ag^+ + e^-$$

The Standard electrode potential of the redox pair above is $E^0 = +0.22V$ in reference to a standard hydrogen electrode. Since it is the same for both electrodes a current can flow through the liquid as soon as a non 0 voltage bias is applied.
The graphene tunneling contacts do not have the capability to undergo reduction/oxidation processes, however the water in the direct vicinity is. The two reactions in an acid milieu

$$\begin{aligned} 2H^+ + 2e^- &\rightarrow H_2(0V) \\ 2H_2O &\rightarrow O_2 + 4H^+ + 4e^-(+1.23V) \end{aligned}$$

and an alkaline milieu

$$\begin{aligned} 2H_2O + 2e^- &\rightarrow H_2 + 2OH^-(-0.83V) \\ 4OH^- &\rightarrow O_2 + 2H_20 + 4e^-(+0.40V) \end{aligned}$$

start as soon as the voltage bias exceeds $1.23V$.

Oxygen in statu nascendi is very likely to destroy the carbon electrodes by oxidation. Besides the current through the liquid will soon increase beyond the nA scale which will make tunneling current measurements more difficult. Therefore all experiments should be performed below the electrochemical threshold of $1.23V$. In the case that there are no reduction/oxidation processes possible, the coupling between the regime of ionic and electronic conduction is exclusively capacitive and described by *constant*

phase angle impedances with the impedance

$$Z(\omega) = \frac{K}{(i\omega)^{\beta}} \tag{3.31}$$

K is some constant and β an exponent between 0 and 1. For most systems with water and an inert metal like gold or platinum the value of β is around 0.8 or 0.9 [8] [75]. The behavior of electrode-electrolyte interface has been subject to intense empirical study and is still not fully understood. First measurements date back to 1900 [127] and continue until the 30ies of the 20th century [27] [46]. It took the physics community quite a while to accept the power law shape of the electrode/electrolyte interface. The exponent β is currently explained by a non-smooth and fractal surface topology of the electrode material [6] [68] [47].

Electrochemical interfaces experience very characteristic $1/f^{\alpha}$-noise. If the mass transfer in the vicinity of the electrode is related to an electric field, $\alpha = 2$. In diffusion dominated regions, ion diffusion creates a noise spectrum with $\alpha = 1$ [34].

3.5 Measurements

Without a molecule between the electrodes the tunneling current can be estimated as $I = \frac{2e^2}{h}TV$ and $T = \exp(-2d\sqrt{2me\phi_0/\hbar^2})$ where V is the bias, e is the electron charge, d is the electrode spacing of about $1.5nm$ and ϕ_0 is the work function of graphene of $5eV$[9]. Lagerqvist et al. find a value of $I \approx 0.1aA$ for vacuum tunneling [57]. A few typical values of tunneling currents in different liquids are given in tab. 3.1.

The current thermal noise, *Johnson-Nyquist-Noise*, from the finite sampling frequency [44] [90] [94]:

$$\delta I = \sqrt{4k_B T \Delta f / R}$$

where T is the temperature, Δf is the sampling rate and R is the resistance of the nucleotide, can be quite important. At a sampling frequency of $\Delta f = 100kHz$ the root mean square current thermal noise is of the order of $40fA$ for Guanine which is still

[9] The equation $I = \frac{2e^2}{h}T(\phi_0)V$ is a limit of Simmons' model for small voltages and a small area/distance^2 ratio. It can be found by a Taylor expansion of equation 3.10 to first order in V.

very small [57]. Noise due to the ionic environment have been measured previously but just for large liquid/electrode contacts with bulk materials [132] [69]. Successful measurements with graphene as electrode material for cyclic voltammetry indicate that noise in the water contact should be controllable [2].

Chapter 4

Experiment

4.1 Graphene characterization

In the project we used graphene from chemical vapor deposition (CVD). The recipe is given in the last part of the thesis. Obtaining a single-layer piece of graphene using exfoliation is a random process, whereas controlled CVD growth of graphene is possible on a large scale [65] [98]. We grow graphene from methane on copper foil at $1050°C$ and ambient pressure. Methane is carried by forming gas, a mixture of 10% hydrogen in argon. The growth of graphene on copper substrates starts with hexagonal single crystals equally distributed that finally merge to a polycrystallene layer of graphene. The three pictures in fig. 4.1 from optical microscopy show the growth of graphene under the same conditions for different times. The hexagons from single layer graphene grow in size until $\approx 10\mu m$. If they grow beyond this critical value a second layer starts growing in the middle of the hexagon while the crystal further increases in size. Then a third layer starts growing and so on. Finally the graphene crystals will merge to a dense and polycrystalline film from single layer and more-than-one-layer graphene.
Stacking of graphene layers is very characteristic for growing in atmospheric pressure. Growing graphene in vacuum results in almost 100% single layer, however it is very difficult to grow hexagons in vacuum. In vacuum graphene grows in flower like structures. Growing graphene at higher temperatures ($1050°C$) makes it more uniform. Also the relative fraction of multilayer graphene increases if the growth in done at lower temperatures. Therefore we try to grow graphene close to the melting temperature of copper[1].

[1]The melting point of copper is about $1080°C$.

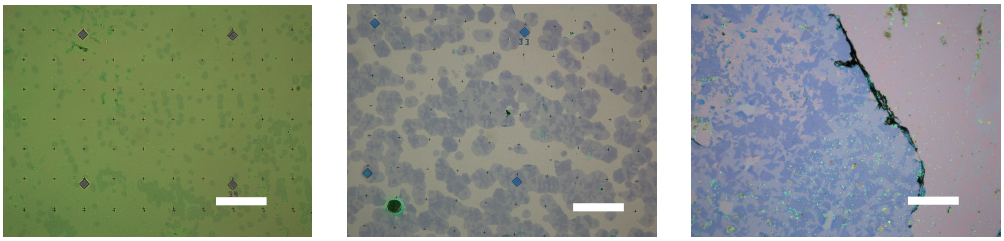

(a) 15 min (b) 20 min (c) 30 min

Figure 4.1: CVD growth of graphene at $1050°C$ from 200ppm Methane in a $10\%H_2$ and $90\%Ar$ atmosphere on copper. The copperfoil has been annealed for 3h at $1050°C$ and methane was added for the the indicated timespan. After the growth, the copperfoil cools down in the $10\%H_2$ and $90\%Ar$ atmosphere. The pictures are optical images taken from graphene transfered to a silicon wafer. The scale bars are $100\mu m$. **a**, Growth for 15min. The visible patterns are alignment marks for lithography. **b**, Growth for 20min. **b**, Growth for 30min.

One method to estimate the quality of graphene is Raman Spectroscopy. A number of very characteristic peaks is associated with graphene. Those lines are called G and D and their respective overtones. G appears from the Raman active E_{2g} phonon, an in plane optical mode. It is located around $1582cm^{-1}$. Its first overtone is referred to as G', located at $3248cm^{-1}$. The width of G depends on the number of layers. D is the honeycomb breathing mode and accessible from elastic backscattering from defects. It is located around $1350cm^{-1}$ and its overtone D' located around $2700cm^{-1}$. The relative strength of D' to G depends on the amount of disorder. The number of layers can be estimated from the width of D' [30] [21] [22]. A sample spectrum of the graphene used here is given in fig. 4.2. It is obtained with a Renishaw inVia Raman microscope at a wavelength of $514nm$. The spots measured are from the sample shown on fig. 4.1a and fig. 4.1c.

Another method to measure the quality of graphene is by using a TEM. As Kim et al. [50] suggested it can be used to map grain boundaries of graphene. Grain boundaries appear naturally if the single crystal hexagons grow in size until they merge with each other. Fig. 4.3 shows the diffraction of the an electron beam if a single grain is illuminated and if a grain boundary is illuminated. The particular picture was obtained from the same growth as the graphene on fig. 4.1c but transfered onto a thin silicon nitride membrane. The TEM grid with the graphene is shown in fig. 4.7.

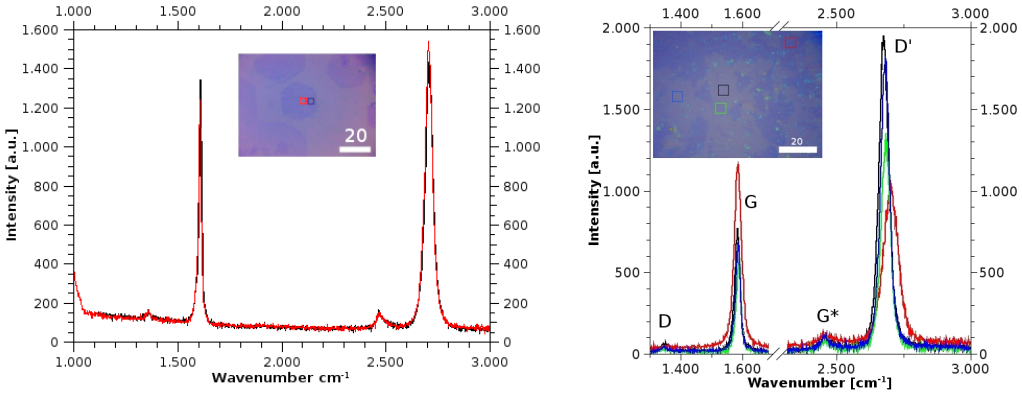

(a) (b)

Figure 4.2: Raman spectra of CVD graphene. The insets are $20\mu m$. **a**, Raman spectrum of single crystal graphene hexagons from fig. 4.1a. The spectrum was taken with a Renishaw inVia Raman microscope at 514nm. The inset indicates at which point of the hexagon the spectrum was taken. **b**, Raman spectrum of a dense layer polycrystalline graphene.

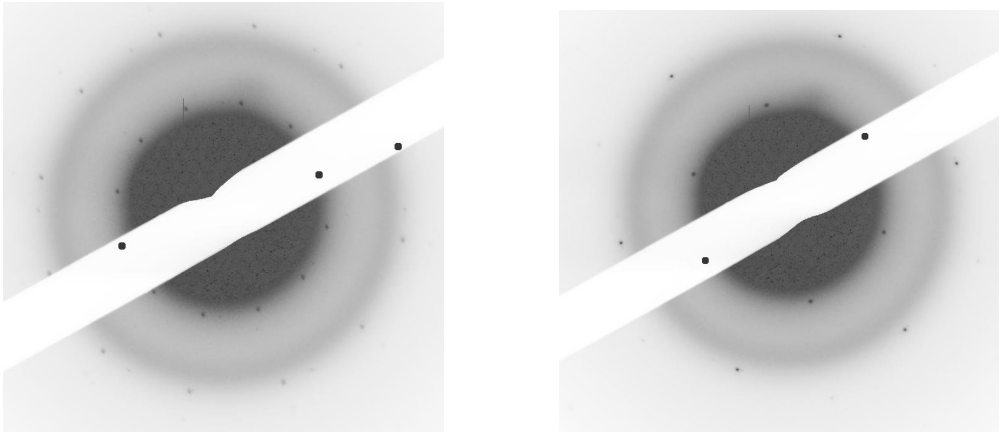

(a) (b)

Figure 4.3: Interference pattern from CVD graphene on a silicon nitride membrane with a JOEL 2010 transmission electron microscope. The alignment software of the JEOL 2010F that was used for these pictures is not working properly therefore we cannot show a correct scalebar. We added hidden diffraction spots which were blanked. The concentric circles are diffraction from the silicon nitride substrate. **a**, Illumination across a grain boundary. The two graphene grains are aligned close to 30° which makes the diffraction pattern look like a 12 point symmetry. **b**, Illumination of a single grain of graphene. In this case just the hexagonal pattern is visible.

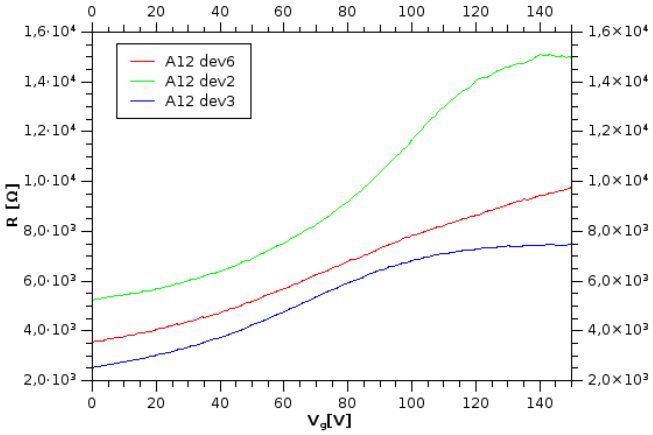

Figure 4.4: Transport measurements of 3 devices on chip A12. The devices are indicated as device 2, device 3 and device 6. The Dirac point of this particular sample seems to be located at about 140V gating. It is the only sample where we could find a maximum in resistance as a function of the gate voltage. All samples which we measured have been p-doped.

Although the CVD graphene seems to be of good quality, the doping levels are very high. We measured transport on about 35 different devices on 7 samples, all cleaned for more then 12h in forming gas at $230°C$ and a Dirac Point was observable just in one case. This case is shown in fig. 4.4. A gate voltage of $V_g \approx 140V$ has been applied to find it. We explain the high doping of our graphene samples by water that has been trapped underneath the graphene. The wet transfer technique, that is described in the methods part, could be to blame for residual water. Although it seems to be a plausible and straightforward explanation, we do not have any evidence for it. Water is a p-dopant for graphene and shifts the Dirac point to positive gating voltages [67].

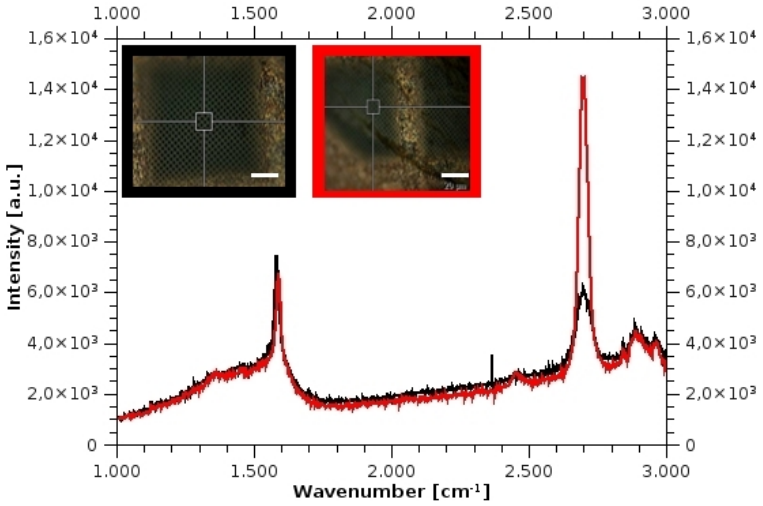

Figure 4.5: Raman spectra of graphene on a TEM grid. Spots with dense graphene and without graphene can be found. The insets show the spots on a TEM grid where the Raman spectra have been taken. The structure at about $1500cm^{-1}$ is the signature of amorphous carbon. It is not visible in the previous spectra. The TEM grid used for this picture is made from an amorphous carbon foil on a copper grid. The scale bar of the insets is $20\mu m$.

4.2 Fabrication of Nanostractures, namely Gaps and Tips

4.2.1 Manipulation in a TEM

We started nanofabrication of graphene using a TEM because e-beam and optical lithography methods do not have the necessary resolution to manufacture devices on single-nanometer scale. We used a DuraSiN Grid[2] and Holey Carbon Grids[3]. DuraSiN Grid are 30nm thick free standing Silicon nitride membranes on a silicon bulk carrier. Holey Carbon grids are made from a holey amorphous carbon film on copper foil. The CVD-graphene was transfered from the copper foil as described in [97] and characterized with Raman spectroscopy. A sample picture is given in fig. 4.5. It is easily possible to identify graphene regions by Raman Spectroscopy as well as by optical microscopy.

[2]Commercially Available by Electron Microscopy Sciences. We used the product DTF-030523.

[3]Commercially from Quantifoil.

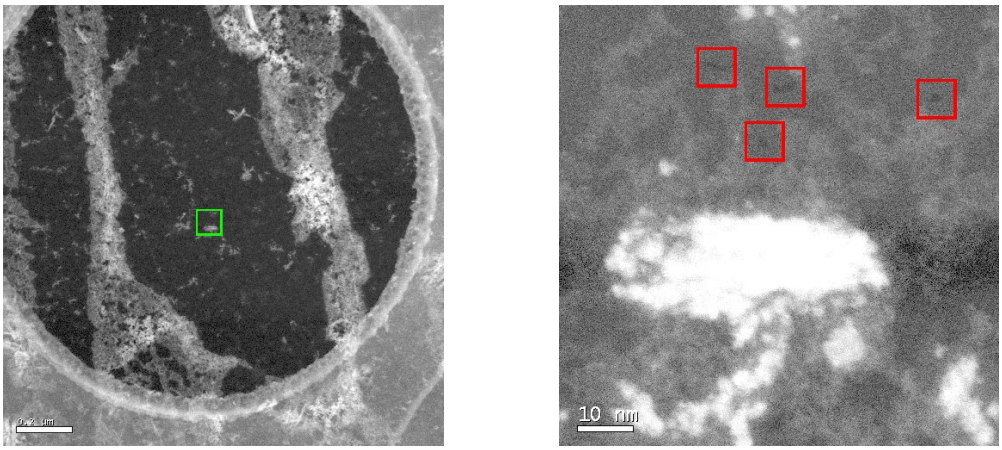

(a) (b)

Figure 4.6: Here we show an example of how we manipulated suspended graphene with a TEM. **a**, Low magnification picture of a hole in a TEM grid covered with a large piece of suspended graphene. Well visible is dirt on the surface of the graphene. The scale bar is $0.2\mu m$. **b,** A high magnification picture of the green box in picture a). We placed the electron beam in the red boxes for about 2min. A change in the surface structure is visible. The scale bar is $10nm$. The beam energy of the JOEL 2010F is 200keV.

Graphene can, as most materials, be modified in a TEM. Lithography methods involving TEMs as TEBAL, Transmission Electron Ablation Lithography [23] are promising methods to produce nm scaled structures on a TEM grid. They work by removing material from the surface of a TEM grid using the intense energy of the focused electron beam. We performed imaging and drilled presumably holes in suspended graphene sheets as shown in fig. 4.6. The machine we used is a JOEL 2010F TEM/STEM located in the Nanophysics Laboratory. We reproduced results previously reported on the fabrication of nanoscale graphene structures [79] [84]. The knockout energy of the electron beam necessary to remove carbon atoms exceeds 100keV. Therefore graphene can not only be manipulated it can also be imaged without destroying it. In fact Suenaga et al. were able to image the edge of suspended graphene in a TEM and show the removal of single carbon atoms [117]. TEMs have also been used to manufacture nanopores in silicon nitride membranes.

After successfully manipulating suspended graphene, we subsequently tried to manipulate graphene on a substrate. It turns out to be very difficult because of the poor contrast between graphene and the material underneath in Dark- and Bright-field mode.

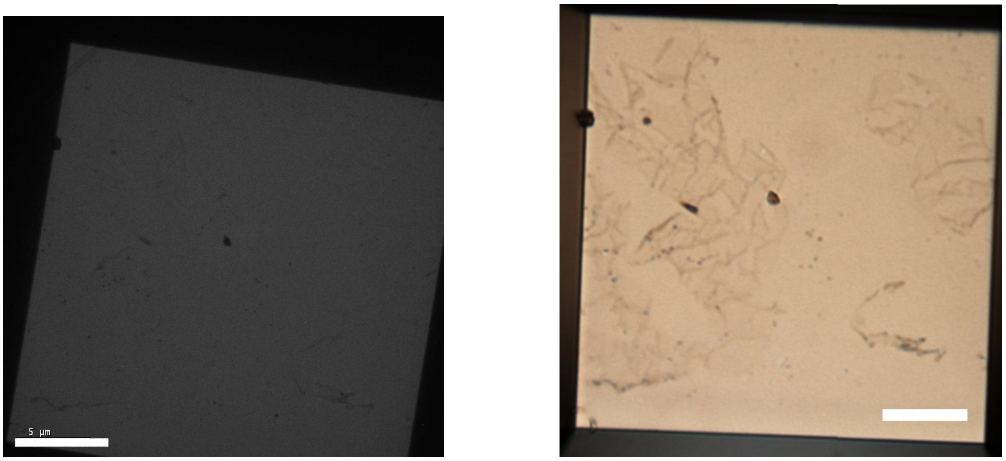

(a) (b)

Figure 4.7: TEM picture of graphene on SiN and an optical image of the same spot. Insets are $5\mu m$. **a**, Shown is a TEM picture in ADF mode of a suspended silicon nitride membrane with CVD graphene transfered to it. Some dust grains are visible but it is not possible to see anything else. **b**, Optical image of the same spot. Some graphene flakes are clearly visible. This figure illustrates the difficulties of imaging graphene on an amorphous substrate with a TEM.

A region of graphene on silicon nitride is shown in fig. 4.7. The pictures show an optical image and a TEM dark-field mode image of the same spot. The difference between both images is obvious. We have not had enough contrast (if any) to find the graphene.
A TEM image obtained in Bragg-Mode can overcome the contrast problems described here: Selecting a single diffraction spot, as those presented in fig. 4.3, in the diffraction plane by a small aperture and imaging of the diffraction spot will make just the parts of the sample visible which contributed to the particular diffraction spot. The so called Bragg-technique has been successfully used to map graphene grains on a substrate in Dark-field mode in a TEM [41].

Considering the difficulties of manipulating graphene on a substrate with a TEM and considering furthermore the complex fabrication of a device on a small TEM grid, we decided to try a much simpler approach to make nanogaps and tunneling probes with graphene: "burning" Graphene in air/vacuum on a silicon chip. This method, described below, turned out to be perfectly suitable with the additional advantage of simplicity and low cost.

4.2.2 Burning tips

Electromigration, a phenomenon caused by momentum transfer between conducting electrons and the atoms of the conductor, is the reason for electrical breakdown in a cable if the current density is too large. Beside the obvious destructive consequences, electromigration has been used to fabricate gaps and tunneling junctions. Electromigration approaches to fabricate junctions on a molecular scale are usually conducted in vacuum and cryostatic conditions [115] [116] [123] [92] but is also possible under crude conditions at room temperature [71]. A good description on electromigration can be found in the PhD Thesis of Jiwoong Park and his advisor Paul McEuen; therefore it is not necessary for us to repeat it [93]. We tried to fabricate graphene tips in a fair vacuum ($5 \cdot 10^{-2} mbar$) and ambient atmosphere at room temperature with an electromigration like procedure:

- Prepare a strip of graphene on a Silicon/Silicon oxide chip and contact it with Au/Ti leads.
- Apply a voltage at the graphene strip.
- Measure the current and calculate the resistance to monitor the forming gaps.

The detailed algorithm is shown in fig. 4.8

Graphene as a conductor will allow current to go through it. This current will heat the sample. One could expect two different processes to occur: First of all, carbon atoms at the edge of a graphene strip are not as strongly bound as those in the bulk, therefore they will oxidize first. We refer to this process as burning. The second process in vacuum is as follows: The carbon atoms at the edge of graphene are weakly bound in comparison with the bulk atoms. Therefore they will evaporate first. However we found no significant difference in tip fabrication between the environments. It could be an indication that electromigration is more important than the burning effect, even in an oxidizing environment.

We used a constant voltage source for the formation of a nanogap. A constant voltage

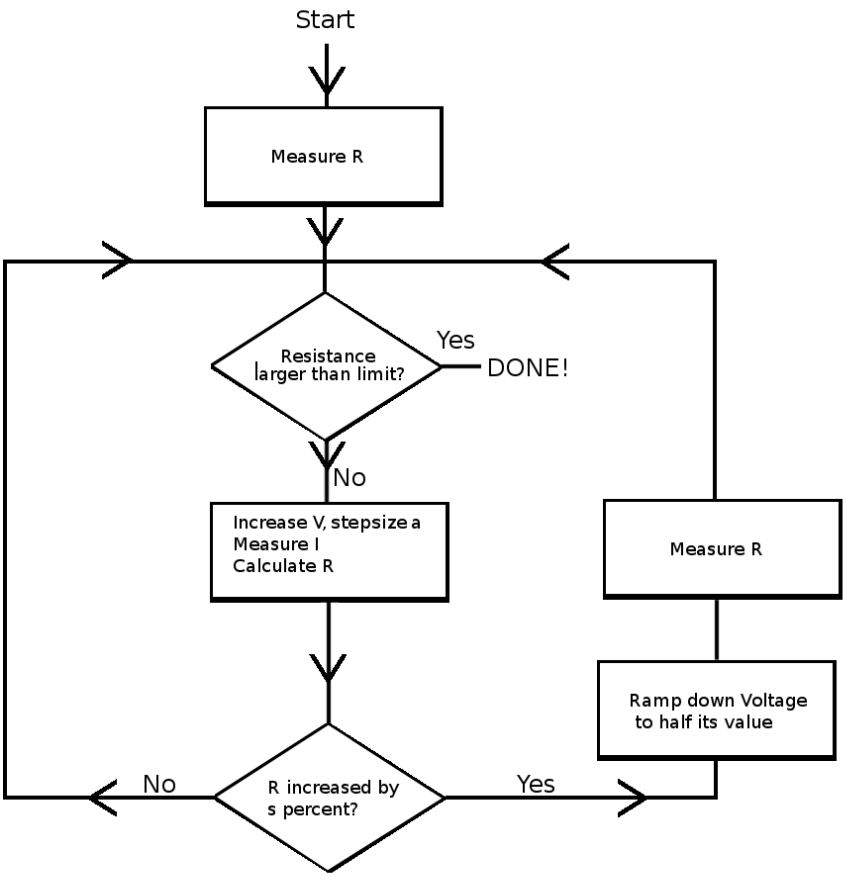

Figure 4.8: Algorithm to form a tunneling junction in a sheet of graphene. It is based on typical electromigration algorithms used to fabricate gold nanostructures. The parameters are the slope of the voltage ramping and the change in resistance s at which the voltage is ramped down again.

source sources a current

$$I = \frac{U}{R} = \frac{U}{\rho l} \cdot A \tag{4.1}$$

so that the current density

$$J = \frac{I}{A} = \frac{U}{\rho l} \tag{4.2}$$

is constant and independent of the width of the graphene strip. With this technique we cannot accidentally burn the graphene if it narrows down rapidly. Thus the gap formation becomes more controllable. Fig. 4.10 shows a typical burning event. As a function of time the voltage is ramped up and down continuously while the resistance is monitored. The resistance as a function of time follows the current, due to its temperature dependence and increases slowly. The time dependence of the resistance is shown in fig. 4.10a. In the parameter space of the current through the sample as a function of applied voltage the point at which the sample is at the moment moves in a zig-zag way. This movement goes continuously toward smaller currents since the graphene strip narrows down. The gap formation process is shown in fig. 4.9. The arrows indicate the movement towards a smaller current/ larger resistance.

This process is shown fig. 4.10b. Remarkably, graphene is tougher than a gold sample with which we experimented to optimize the electromigration-like burning program. The current densities necessary to break gold are a factor of 10 smaller [93].

The result of burning a strip of graphene is shown in fig. 4.11. Fig. 4.11a shows a very volatile destruction of the graphene. In contrast the gap formed at 4.11b is very promising. This gap has a diameter of $\approx 50nm$. It is still to large to measure any tunneling - however easy to see in SEM wherefore we show the image. Very small structures in graphene are extremely difficult to see.

The breakdown current density in our graphene samples is about $5 \cdot 10^{12} Am^{-2}$ assuming a thickness of $0.3nm$. To control the burning process we have worked with single-crystal graphene (hexagons as shown in fig. 4.1a and their Raman spectrum in fig. 4.2a.) and burned the devices usually under fair vacuum conditions with a pressure of $5 \cdot 10^{-2}$mbar.

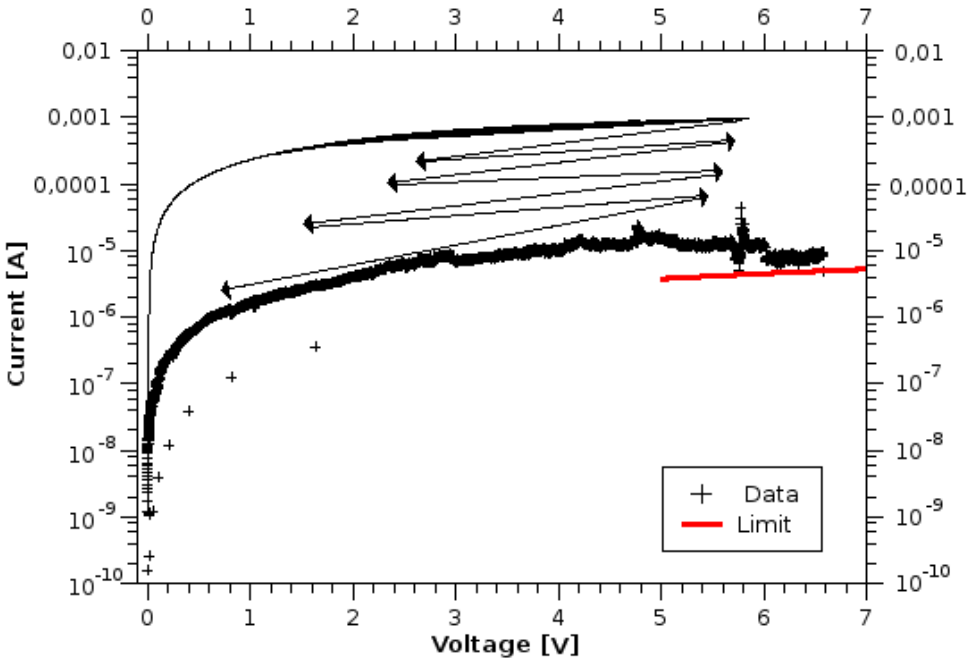

Figure 4.9: Gap formation in a sheet of graphene in the voltage/current parameter space. Ramping up and down the voltage forms a constriction in the graphene which again increases the resistance. Thus the zig-zag motion in respect to the voltage goes continuously towards smaller currents. This motion is indicated with the black arrows. As soon as the resistance hits a limit, which is preset, the voltage is ramped down to 0V and the gap formation process stops. The resistance limit is indicated by a red line.

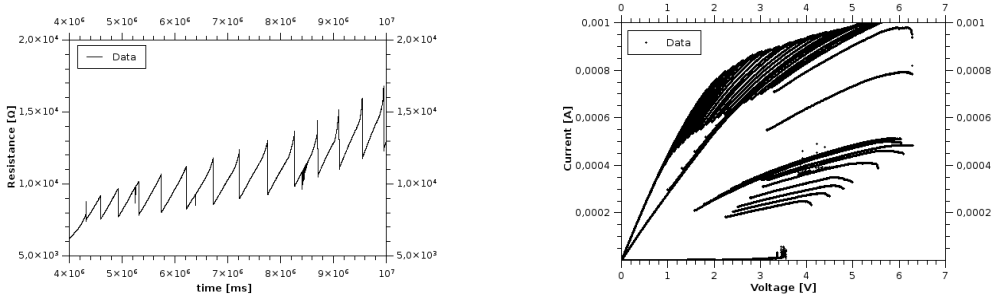

(a) (b)

Figure 4.10: The gap formation process. **a**, Gap formation process as a function of time. The voltage is ramped up and down. The heating of the graphene strip changes the resistance, therefore the ramping is visible in the resistance curve as well. The tendency of the resistance is upwards. **b**, Gap formation process in the voltage-current parameter space. The voltage is ramped up and down, the current therefore goes up and down as well. Due to a change in the resistance the current drops. In the end the curves look like a zick-zack downwards. The breakdown of graphene is very similar to a gap formation in gold.

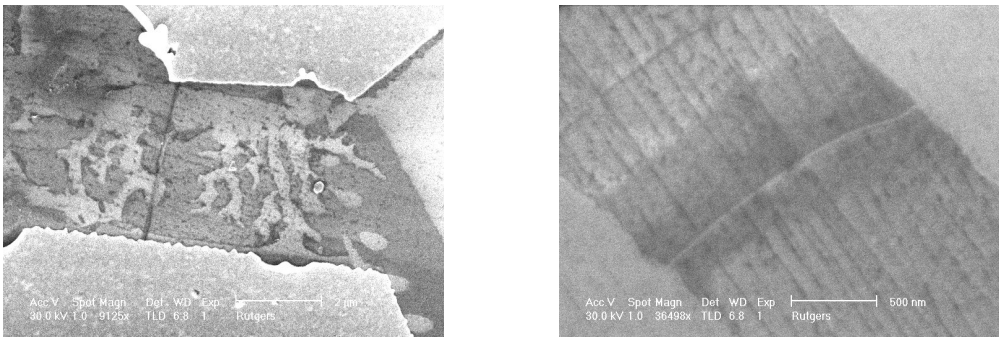

(a) (b)

Figure 4.11: Two SEM pictures of burned graphene sheets. **a**, This picture shows a destructive formation event. The graphene edge is jagged. The graphene used here has been polycrystalline. It was one of the first devices which we fabricated. **b**, This picture shows a smooth gap in a strip of graphene. This particular gap has a size of $\approx 50nm$ which is too large for tunneling but easy to see in SEM.

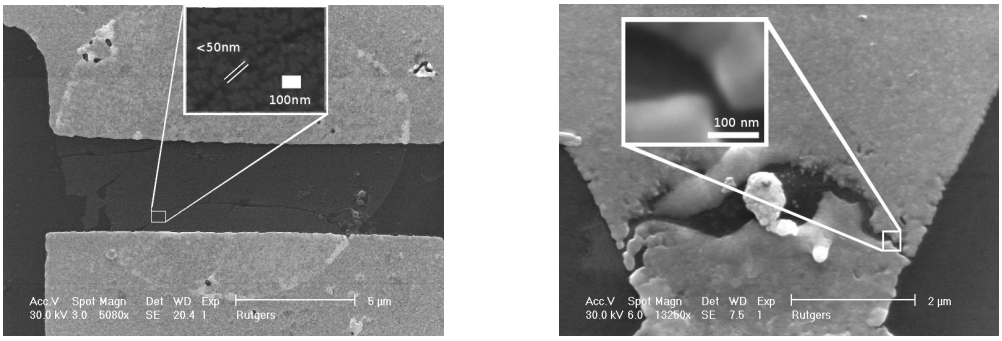

(a) (b)

Figure 4.12: This is how we fabricate graphene nanostructures after optimizing the process. **a,** shows a picture of a graphene hexagon with a very small structure in in. **b**, The same algorithm as for a) has been applied to a gold junction. The tunneling current in this gold junction is 5nA at 1V bias in vacuum.

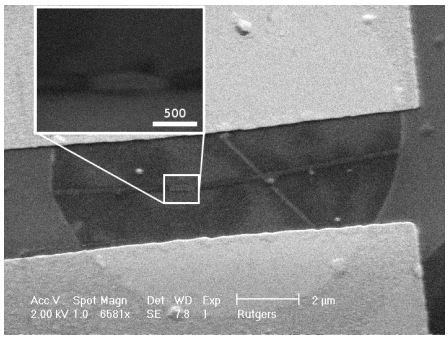

Figure 4.13: To control where a tunneling gap forms we pattern the graphene with a constriction of $\approx 1\mu m$ somewhere using reactive ion etching. After the pattern has been made the graphene device is burned. An example is shown here.

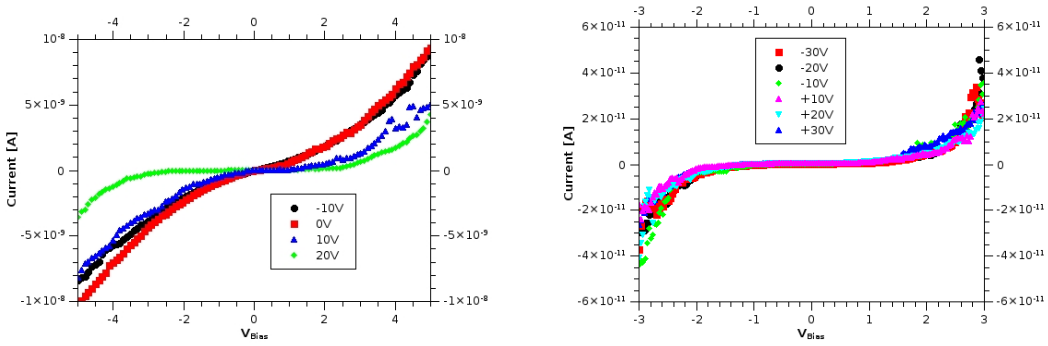

(a) (b)

Figure 4.14: Two tunneling junctions formed in a graphene sheet. **a**, A strong gate dependence is observable. It is not an effect of gate leakage since the curves all go through (0,0). **b**, A graphene tunneling device without a gate dependence. There is also no gate leakage observable in this case.

4.3 Tunneling currents

Once a graphene junction is formed we measure I(U) curves. From the result of the measurement the "dark" current through the probe station is subtracted. This "dark" current arises due to a non perfect insulation and moisture in the environment. It is shown in fig. 5.3 in the chapter on measurements. Two typical voltage/current curves are shown in fig. 4.14. The first picture shows the current with applied gate voltage in air. The second picture is tunneling across a different device where no gate dependence is observable. We explain both curves with the high doping of the CVD graphene. If the graphene is doped high enough it will behave like a metal; a few 10V of gating will not change enough to have an effect on the tunneling curves. If the graphene tunneling junctions has formed at a clean spot, the gating will have an influence to the density of states. If we approach the Dirac Point (with positive gate voltages) the tunneling current should decrease because there are less states to tunnel into. This effect could explain fig. 4.14a.

We could measure tunneling current with a relatively strong gate dependence and almost no gate dependence at all. Those two cases are shown in fig. 4.14. We assume that the high doping of the CVD graphene masks the features of the graphene DOS as the Dirac point so that it appears as a metal. If on the other hand the spot, where the

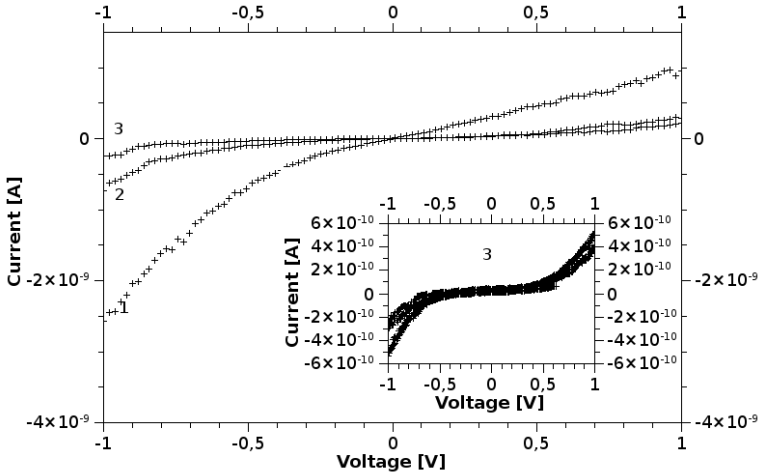

Figure 4.15: Tunneling through vacuum with slowly increasing helium pressure. Curve 3 is the vacuum curve. 2 has been measured with an intermediate helium pressure, 1 at almost atmospheric helium pressure. The inset is a tunneling curve in vacuum, curve 3. We measured the tunneling curve in vacuum three times to show that it is reproducible. The current increases as the helium concentration increases, however the currents are still extremely small. Superexchange makes through bond tunneling more effective than through space tunneling [76]. This effect is observable here.

junction is formed, is very clean, we can find a gate voltage dependence.

Adsorption of molecules from surrounding air and its influence onto tunneling currents has been previously reported [58]. We have therefore tried to measure tunneling spectra in ambient air and vacuum. The HOMO/LUMO gap in nitrogen can be derived from UV absorption spectra where the HOMO/LUMO transition accounts for a strong absorption line. The value is about $2eV$. The van-Hove singularities in graphene also appear at $\approx \pm 2eV$ around the Fermi Level. In principle we should be able to see both, however we have to apply a large voltage to do so. Therefore we decided against a direct measurement of those features and to rely on effects of inelastic tunneling.

Fig. 4.15 shows that the tunneling currents depend on the atmosphere. We can see an increase in tunneling current from $0.1nA$ to about $1nA$ if the measurement chamber is flooded with helium. The effect was very strong in this particular device and much smaller in others. Therefore we are not completely sure that what we observe is a a real effect. However this is the behavior which we would expect from a tunneling junction. An alternative explanation for the voltage current curves we measured could be a gas

discharge between the two pointy electrodes. Graphene vacuum electron emission has been studied before [59]. The work function of carbon is about the same as for gold $W \approx 5eV$. The equation to describe the saturation current of an electrode is Richardson Equation. the two important parameters are the work function W and the temperature T

$$j = c \cdot T^2 e^{-\frac{W}{k_B T}} \tag{4.3}$$

For vacuum emission the voltage current curves are highly non-linear. In a regime not to close to saturation and far enough from $U = 0$

$$I \propto U^{3/2} \tag{4.4}$$

from Poisson's equation

$$\frac{d^2U}{dx^2} = \frac{1}{\epsilon_r \epsilon_0}\rho \tag{4.5}$$

$$\rightarrow \frac{U}{d^2} \approx \frac{ne}{\epsilon_r \epsilon_0} = \frac{j}{v\epsilon_r \epsilon_0} \tag{4.6}$$

where d is the distance between the tips and n is the charge carrier density, and the conservation of energy

$$v = \sqrt{\frac{2e}{m}U} \tag{4.7}$$

For small negative bias voltages the current follows a Maxwell distribution

$$I \propto e^{-\frac{e|U|}{k_B T}} \tag{4.8}$$

because just the electrons from thermal emission which can overcome the voltage produce a current. Both graphene tips should have the same temperature, so this is not an issue here. A gas discharge has a voltage current curve which is

$$I \propto U \tag{4.9}$$

for small bias voltages. If the bias voltage increases a saturation effect occurs and the current will not increase further. If the voltage increases even more the current increases rapidly by secondary ionization effects in the gas. It is difficult to distinguish between

an ionization or field emission effect, as eqn. (4.4) and (4.9) and tunneling in air and other gases however there should be no such effect in a liquid. The voltages which we apply are too small to ionize molecules of the liquids[4]. To check the I(U) curves of both liquids and gases we perform fits to Simmons' model. If the fits work out, we refer to them as tunneling curves.

We also found a type of voltage current characteristic which is exponential over a large scale. An example is shown in fig. 4.16. Measurements like this one have been described by S. Shin et al. [109]. They attribute a signal as

$$I = I_0 e^{\frac{|U|}{U_0}} \tag{4.10}$$

to strong disorder in the graphene introduced by the large current density in the gap formation process. To analyze the degree of disorder they perform Raman analysis of their graphene samples where they can find evidence for spatially localized regions with a high degree of disorder.

In this thesis we fabricated devices which seemed to be potential tunneling candidates (almost no transport across the graphene after the burning process) but those samples looked perfectly fine in optical microscopy and in SEM. If there were to be a gap it has to be smaller than the resolution limit of SEM. On the other side we can attribute the exponential behavior of the graphene devices to the introduction of disorder into graphene: It will not change the optical appearance however it will increase the resistivity by orders of magnitude.

At this point we are not sure why some samples form narrow regions where graphene is removed and others form regions with allegedly strong disorder. A sample where we can find an exponential current/voltage curve is shown in fig. 4.16

[4]Ionization in this context is equivalent to electro-chemistry.

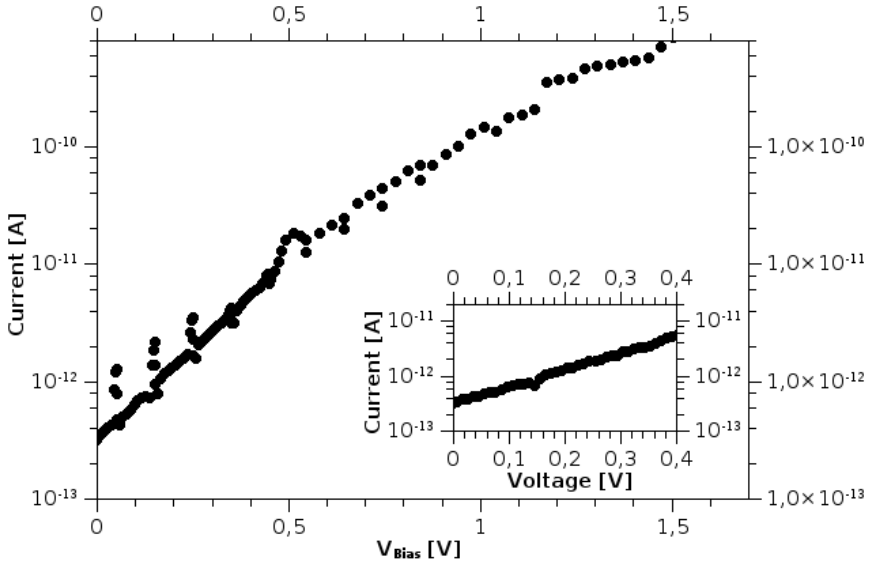

Figure 4.16: A disordered phase in graphene can allegedly be induced by a large current density as Shin et al. show [109]. The inset is a magnification and seperate measurement of the first part of the curve. Strong disorder can explain a current $I = I_0 e^{\frac{|U|}{U_0}}$.

4.4 Nanochannels

4.4.1 Transport and Electrochemical aspects

To embed a graphene electrode in a nanoelectrode we first fabricate nanochannels by e-beam lithography: A sacrificial gold structure on Silicon oxide was buried in PMMA or Al_2O_3. The gold structure was etched and an open channel remained. To contact the nanochannels we used Ag/AgCl electrodes which we fabricated as described in the methods section of this thesis.

Fig. 4.17a shows a Voltage/Current curve of a still closed nanochannel. As soon as the bias voltage exceeds $1.23V$ electrochemical processes between gold and water can occur and the goldbridge in water becomes conductive.

Something similar can happen if there is no AgCl covering the negative pole of the electrodes and the nanochannel is open. Then the process $Ag^+ + e^- \rightarrow Ag$ cannot take place. Those electrodes show a behavior as in fig. 4.17b. As soon as the bias voltage reaches $0.8V$ a current starts flowing due to $2H^+ + 2e^- \rightarrow H_2$ instead of $Ag^+ + e^- \rightarrow Ag$ as cathode reaction.

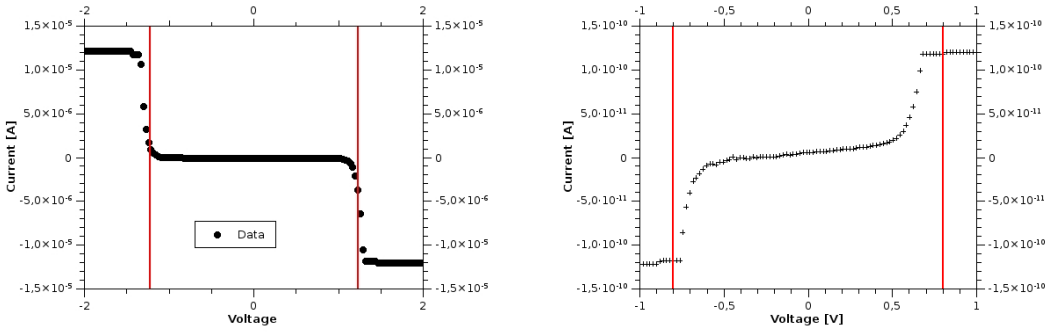

(a) (b)

Figure 4.17: Effects of a blocked nanochannel and an insufficiently prepared silver electrode. **a**, If the nanochannel is blocked with gold, electro-chemistry can take place as soon as the voltage exceeds 1.23V. The red lines indicate $\pm 1.23V$. The plateaus at the end of the curve account for the end of the measurement range of the current amplifier. **b**. A different problem is if the electrodes are not covered with AgCl. Then the cathode reaction $Ag^+ + e^- \rightarrow Ag$ is not possible. The bias voltage needs to exceed 0.8V to allow $2H^+ + 2e^- \rightarrow H_2$ instead. That is the problem here. 0.8V is indicated with the red line. The plateaus at the end of the curve are again an artefact of the current amplifier.

As soon as the gold of the sacrificial layer is etched entirely and the silver electrodes are well prepared a current across the nanochannel can be measured. This current helps to estimate the geometrical properties of the nanochannels.

Fig. 4.18a shows transport across a nanochannel device compared with transport through bulk liquid. The red curve is magnified in fig. 4.18b. It corresponds to a resistance of about $17G\Omega$. This particular nanochannel is $20\mu m$ in length, about $200nm$ in width and $50nm$ in height. It is shown as an example in the methods section in fig. 6.8. The length and the width have been measured on the gold sacrificial structure in the SEM prior of burying everything in Al_2O_3. The height is well known from the metal evaporation process. From the resistance we can estimate the resistivity of the electrolyte given the geometry of the canal. The result is $\rho = 8.5\Omega m$. The literature value of 2M potassium chloride solution is around $0.05\Omega m$ and depends on the temperature[5]. We are off by a factor of 100. An obvious reason could be that there is still some gold remaining in the nanostructure. However we saw no evidence for any

[5]"Conductivity: Theory and Practice", Radiometer analytical - A Manual on measurements in electrolytes and a collection of tables.

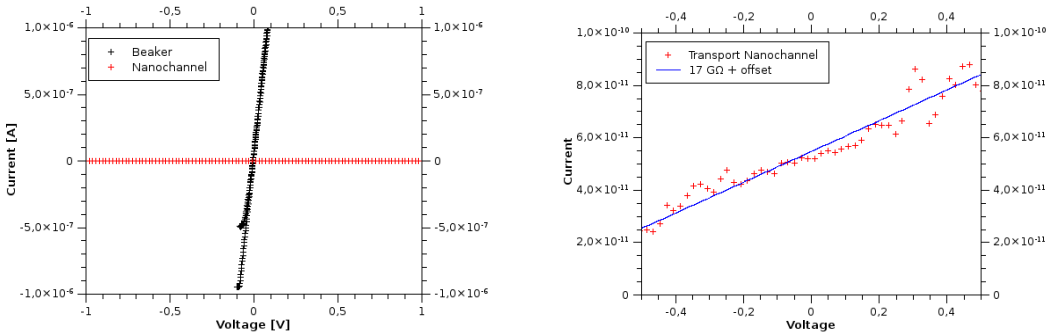

(a) (b)

Figure 4.18: Ionic conductance along a nanochannel. **a**, Transport from a Ag/AgCl electrode to another if both are placed in a beaker with a good electrolyte is shown in black. There the conductance is very high. If those electrodes are connected with a nanochannel there is still transport measurable, however the resistance of the nanochannel is extremely large due to its length and its extremely small cross section. Current along the nanochannel is shown in red. The electrolyte is 2M potassium chloride in water. **b**, A magnification of the red curve from figure a). The fit is a linear fit with $17G\Omega$ and a constant offset.

left gold in optical microscopy on this device. The device was kept in gold etchant for 24h which should be enough to remove all gold. Another reason could be the wetting behavior of graphene with water: Graphene is highly hydrophobic. It will therefore repel water and the ions within water effectively. This effect can hold for an increase in resistance of the nanochannel. Another explanation could be a trapped bubble of air in the nanochannel. As an effect of the extremely small cross section of the nanochannel, even the tiniest bubble or grain of dust will increase the resistivity by a large factor.

4.4.2 Tunneling in a nanochannel

To measure a nanochannel device in respect to tunneling we used a probe station. First we measured the dark current through the current amplifier system. This background has been subtracted from the voltag-current curves of the devices. An example of both graphs is shown in fig. 4.19. The difference is fitted to Simmons' model as shown in fig. 4.19b.

We measured the barrier height of graphene to air, water, isopropyl alcohol, acetone and ethanol. The results are shown in table 4.1.

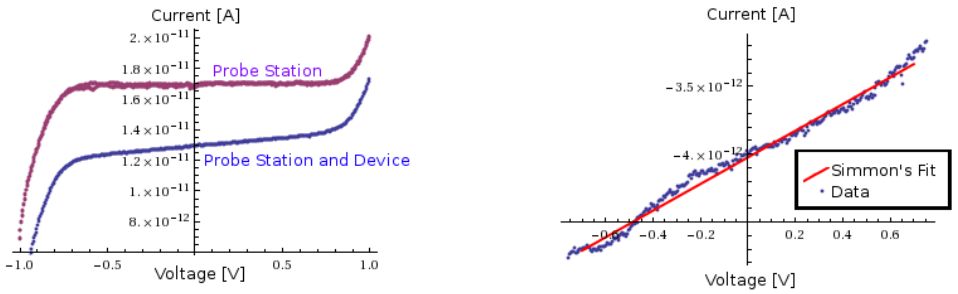

(a) (b)

Figure 4.19: The fitting technique we used. **a**, Plot of the tunneling current (blue) and the dark current through the setup (purple). **b**, Both are subtracted give the blue dotted line. This is the data to which the fit with Simmon's model is done. The fit is the red line.

Substance	ϕ_0 (Gold)	ϕ_0 (graphene)	Distance	Area
Air	-	2.1(1.5)eV	1.0(0.2)nm	$2.1 \cdot 10^{-19}(\dot{-}10)m^2$
Air	-	2.3eV	0.8nm	$1.3 \cdot 10^{-20}m^2$
Water	0.93eV	2.1eV	1.1nm	$2.4 \cdot 10^{-18}m^2$
Isopropanole	1.68eV	1.8eV	1.4nm	$1.2 \cdot 10^{-17}m^2$
Acetone	-	1.3eV	1.3nm	$2.1 \cdot 10^{-18}m^2$
Ethanol	1.54eV	2.45eV	0.27nm	$6.4 \cdot 10^{-19}m^2$
Water	0.93eV	2.8eV	0.8nm	$4.5 \cdot 10^{-16}m^2$

Table 4.1: The table shows the fit parameters to all tunneling curves obtained so far. The values for gold are literature values shown for a comparison [96]. The first 5 lines are fits to a nanochannel device. The line below is a fit to data on a blank graphene device exposed to ethanol. The last line is a fit to a different graphene device exposed to water. The number in brackets in the first line indicates the error.

A problem is that we can neither control the geometry of the tunneling junctions nor measure it. Therefore the Simmons' fits have three free parameters, the work function, the distance and the effective area. That makes the error bars quite large. Since ϕ_0 and d enter in the exponent their error is smaller than the error of the area A. The error of the work function ϕ_0 is about $1.5eV$ for all samples. The error of d is about $0.2nm$ and the error of in the area is a factor of 10. It is quite the same for all fits. Graphene is $\approx 0.3nm$ thick so that we would expect a few times $10^{-20}m^2$ as a typical cross section of a pointy graphene structure. The barrier heights also have the right order of magnitude. The distance of the graphene tips is very small which could be an effect of the electromigration-like burning process: As soon as a gap forms, the current decreases by orders of magnitude and the gap cannot increase in size.

Although we cannot measure the work function of graphene to different liquids with high precision we have reason to assume that we can indeed form tunneling junctions and measure tunneling through different solvents. We have subsequently tried to measure molecules diluted in water with the nanochannel device. Fig. 4.20 shows 5 different measurements of 50μ molar Rhodamine B diluted in water with the same device. We can find plateaus in the spectra which seem to be reproducible. For a comparison tunneling through water is shown.

The positions of the plateaus is listed in tab. 4.2 and compared with features of water and Rhodamine B in IR absorption spectroscopy. Since the energies are too small to be an effect of HOMO/LUMO transitions we attribute the plateaus to an inelastic tunneling effect. Measuring a tunneling curve takes a few minutes so that we see a time average of water and the diffusing Rhodamine molecules. The plateaus at $-0.5V$ and $0.38V$ can be found in both measurements[6] in fig. 4.20a and fig. 4.20b. The lines at $-0.17V$ and $0.09V$ can just be found in the Rhodamine experiment. The plateau at $0.5eV$ could correspond to the strong absorption lines of water around $4000cm^{-1}$. That explains why we can measure a plateau-like structure at this point in both experiments. Water however does not have a feature at $\approx 3000cm^{-1}$. This is a typical scale of a CH

[6]The different amplitudes of the tunneling current in both pictures are likely to be caused by a different device geometry.

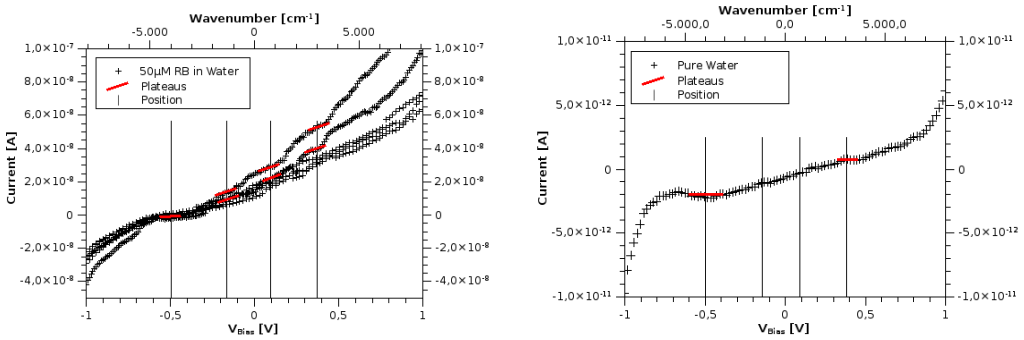

(a) (b)

Figure 4.20: A comparison on tunneling in a device filled with water and another device filled with a 50μ mol Rhodamine B in water. **a**, Five different tunneling spectra of a nanochannel device filled with 50μM Rhodamine B in water. We find a few plateaus which we indicate by red lines. The corresponding energy scale is indicated with the black lines. There are plateaus which seem to be reproducible on a varying background. Since we work with water of limited purity it is not surprising to have electrochemical processes which can account for the varying background. **b,** Tunneling though water without Rhodamine B. The black lines indicate the plateau positions from fig. 4.20a. The red lines indicate plateaus which can be found in this plot. It seems that the innermost plateaus at $-0.17V$ and $0.09V$ are no longer visible.

stretching vibration. Being optimistic we can explain this feature by a hydrogenated graphene edge. The feature at $0.17eV$ could be caused by Rhodamine B. It has many vibrational excitations around $1300cm^{-1}$ as shown in fig. 4.21b. The faint structure at about $90meV$ could be related to Rhodamine B since water does not have any vibrational modes associated with this number. We can find a few lines around $650cm^{-1}$ in the Rhodamine spectrum.

A very common technique of identifying inelastic tunneling is taking the second derivative [111], however our data is too noisy which makes a numerical second derivative extremely difficult. Therefore we rely on the quite crude technique of comparing plateaus with IR spectroscopy. The IR spectral data for Rhodamine B is copied from Farag et al. [20]. The absorption spectrum of air[7] in fig. 4.21 shows how particularly strong the feature of water around $4000cm^{-1}$ is.

We performed the same experiment with Adenosine monophosphate which is one of

[7]Measured with a Vector 33 Fourier Transform Infrared Spectrophotometer, Bruker Biospin Corporation

Peak Position	Wavenumber	FTIR Spectrum comparison
-0.5V	$4030cm^{-1}$	$\approx 4000cm^{-1}$ (water)
-0.17V	$1370cm^{-1}$	$\approx 1300cm^{-1}$ (Rhodamine B)
0.09V	$730cm^{-1}$	$\approx 650cm^{-1}$ (Rhodamine B)
0.38V	$3064cm^{-1}$	$\approx 3000cm^{-1}$ CH-stretch?

Table 4.2: Plateau positions from tunneling with $50\mu M$ Rhodamine B. The first three features can be found in the IR spectra of the molecules. $3000cm^{-1}$ is a typical value for the CH-stretch mode in an organic molecule [91].

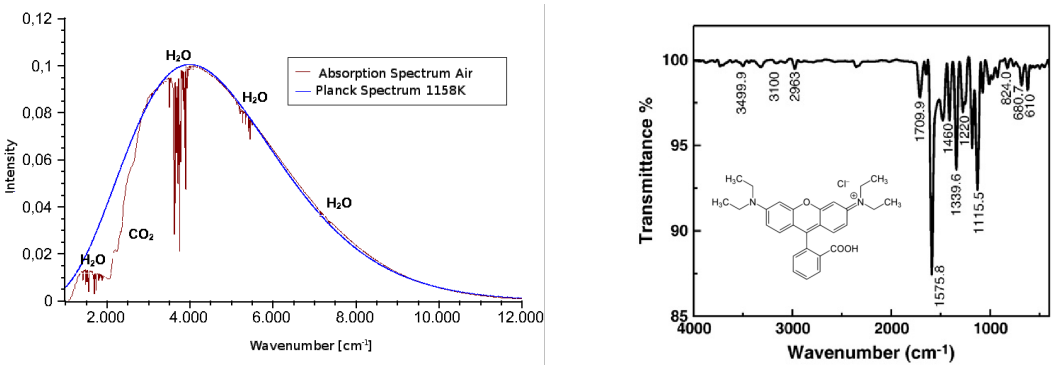

(a) (b)

Figure 4.21: Optical spectroscopy data of water and Rhodamine B. **a**, Spectrum of light emitted from a black body with a temperature of $1200K$ after transmission through air. The very typical vibrational excitations of water around $4000cm^{-1}$ and $1200cm^{-1}$ are indicated and easy to see. There are also some minor features of CO_2 around $2200cm^{-1}$ which we could not find in the tunneling measurements. **b,** The IR absorption spectrum of Rhodamine B is copied and adapted from Farag et al. [20]. The inset shows the structure of Rhodamine B.

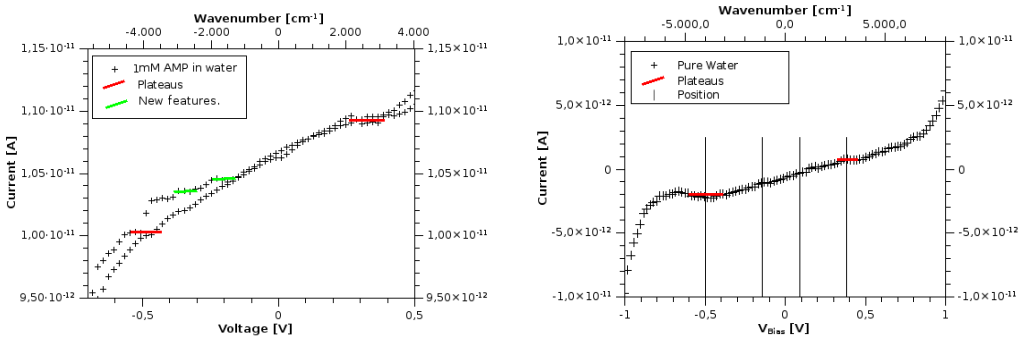

(a) (b)

Figure 4.22: Analysis of 1mM AMP solution in water. There are features visible which cannot be detected in the pute water curves. AMP does have a stron feature around $3000cm^{-1}$ [53].

the four building blocks of DNA diluted in water. The result is shown in fig. 4.22.

We can find additional features in respect to water which can be correlated with vibrational excitations of AMP [53]. The result of this analysis is that we can find structure in the tunneling curves of nanochannel devices which could be related to a characteristic molecule. However we do not have enough statistics to be convinced about it.

Chapter 5

Measurement Setup

5.1 Experimental Setup

The following chapter is dedicated to the measurement system. It contains the measurement setup and the interface software.

5.1.1 Description of the System

A device which we want to measure is placed in a probe station, a setup equipped with a microscope, stainless steel and electrolyte contacts and micromanipulators to place them on a sample. Besides there is a number of measurement devices and a computer equipped with Labview to control the system. A picture of the probe station is shown in fig. 5.1. Fig. 5.1a shows the entire probestation and fig. 5.1b the central part where a device is contacted. This part is wrapped in aluminum foil in fig. 5.1a.

Measurements are also possible with Ag/AgCl electrodes in potassium chloride solution. With this setup the measurements along a nanochannel have been performed.

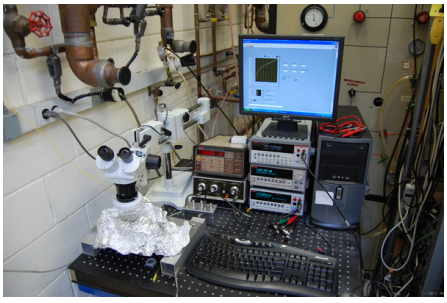

(a) Probe Station

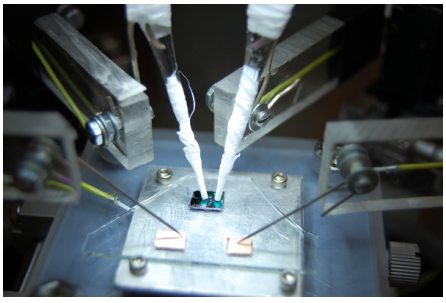

(b)

Figure 5.1: The ambient conditions probe station. **a**, A picture of the probe station with the sample holder wrapped in aluminum foil. **b**, A contacted nanofluidic chip in the probe station.

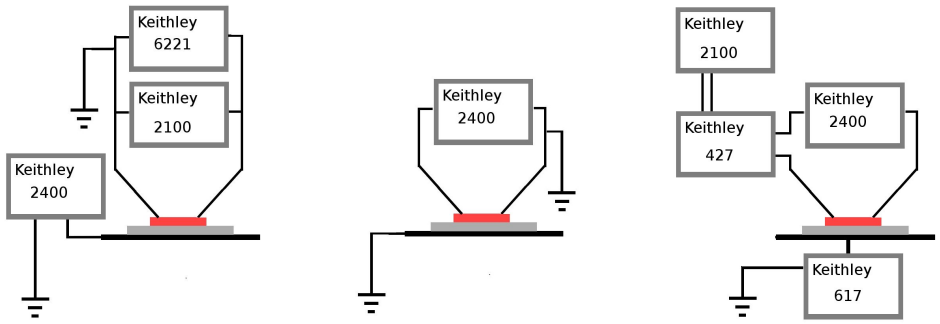

(a) (b) (c)

Figure 5.2: Different measurement modes realized with the probe station. The gate plate is shown in gray, the sample in red. **a**, The setup for transport measurements. **b**, The setup for burning tips. **c**, Setup for measuring tunneling spectra.

Low Level measurements require a shielding of the device. A simple solution is wrapping the sample holder in fig. 5.1b in aluminum foil and grounding the aluminum foil. The triboelectric effect requires not to touch anything while measuring because any movement triggers a charge separation in the coax cables[1]. Measurements in vacuum and different gases can be performed if the sample is wirebonded and placed in a small vacuum chamber. The lowest pressure achievable with this vacuum chamber is $\approx 2 \cdot 10^{-2}$mbar by a turbopump. The small vacuum/gas chamber is shown in the methods parts in fig. 6.12.

The probe station in its current setup can perform three different programs

- Transport Measurements

  A Keithley 6221 Current Source is used as constant current source for a two terminal measurement. A Keithley 2100 multimeter measures the Voltage drop at the sample. The same time the sample can be gated by a Keithley 2400 sourcemeter. The current through the sample is kept constant and the resistance of it is shows as a function of the gate voltage. The setup is shown in fig. 5.2a.

- Burn Program

  A Keithley 2400 is used as a constant voltage source. The sourcemeter is able

[1] A detailed study of the Keithley Manual on Low-Level measurements has helped us in building the setup [134]

to sense current while sourcing voltage. This ability is used to monitor the sample resistance. The voltage is continuously increased until the sample resistance changes by a predefined percentage. When that happens, the voltage ramps down with a predefined rate and increases again. If the desired resistivity of the device has been reached, the process terminates automatically. The setup is shown in fig. 5.2b.

- Tunnel Current Spectra

  A Keithley 2400 is used as voltage source. The current through the sample is measured with an inverting current amplifier Keithley 427. The output of the amplifier is measured by a Keithley 2100 multimeter in voltmeter mode for high precision measurements or with a National Instruments USB-6008 ADC for a high sampling rate. The setup is shown in fig. 5.2c.

The output signal in the fast tunneling measurements mode is digitalized with a National Instruments USB-6008. The precision of the voltage measurements is 5mV at all sampling rates. The fastest sampling rate possible is 10kHz[2]. The 5mV precision of the Analog/Digital Converter has to be added to the precision of the current amplifier. The results for precision are given in tab. 5.1. A fast and precise current measurement is necessary for single molecule detection as demonstrated by M. Tsutsui et al. [122]. We have tried to find spikes in the current traces in the Rhodamine B measurements but could not find any. Our problem is the insufficient voltage resolution of the USB-6008.

Another important issue is the conductivity of the probe station setup itself which is of the order of a few $T\Omega$. The dark currents through the probe station cannot be removed with a better setup therefore they are always subtracted: Every measurement is performed twice and the difference is shown. If the conductivity of a sample exceeds 10pA or so the current through the probe station is no longer important. The dark current of several measurements without a sample is shown in fig. 5.3. It shows the current from one contact needle to another and the current from one needle to the gate.

Fig. 5.4 shows the dark current of the vacuum/gas chamber. Although it is much

[2]National Instruments Manual USB-6008/6009

Rise Time^{-1}	RMS noise input	RMS noise output	RMS result (Data on computer)
3Hz	2fA	0.2mV	50fA
10Hz	4fA	0.4mV	50fA
100Hz	40fA	4mV	60fA
1kHz	0.4pA	40mV	0.5pA
10kHz	5pA	5mV	7pA
30kHz	400pA	4mV	-

Table 5.1: Possible sampling rates and precisions in the fast tunneling current measurements of Keithley 427 and National Instruments USB-6008. Numbers are from the Keithley 427 Manual and the National Instruments USB-6008/6009 manual.

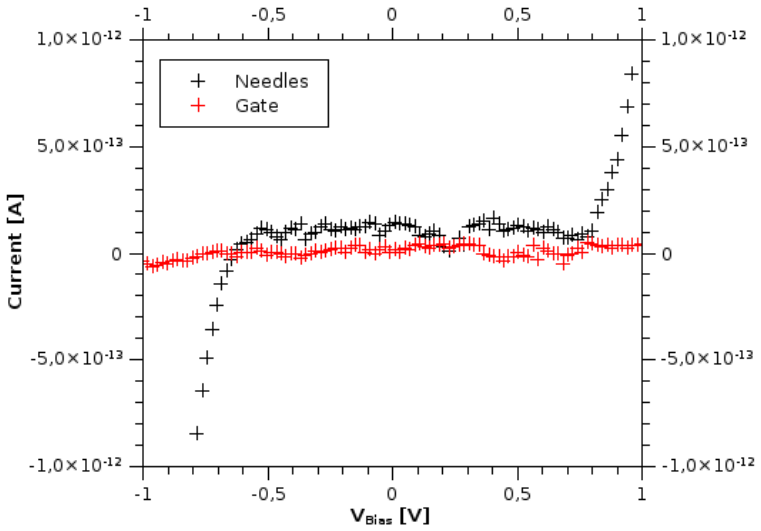

Figure 5.3: Darkcurrent of the probestation.

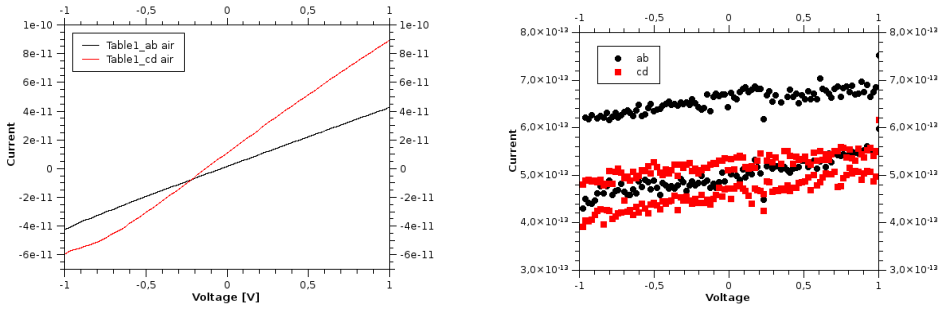

(a) (b)

Figure 5.4: Dark current without a device of the vacuum/gas chamber system. The sample holder has 4 contacts for wirebonding, indicated as A, B, C and D. We used (A, B) and (C, D) to contact a two two-terminal device. Therefore we show the dark current from A to B and from C to D. **a**, Dark current of the chamber measurements in air. **b**, Dark current of the system in vacuum. If the currents are very small, as they are here, there is a time dependence in the background. Both red and both black curves have been measured on two different days. An effect of time dependent background is that we measured the background previous to every measurement.

better in vacuum it is still not as good as the probe station (besides it is not as good shielded: The probestation is contacted with coax cables whereas the vacuum chamber is contacted with twisted pair cables).

5.1.2 Software

The software of the probe station is written in Labview 7.1. The front panel of the gap formation program is shown in fig. 5.5. The front panel for the tunneling spectum programs is shown in fig. 5.6.

Fig. 5.5 shows a graphene gap in the forming process. The voltage has ramped up and down several times so far. The window on the left shows the current resistance, the window on the right shows the current as a function of the voltage. Since the program automatically ramps up and down the voltage, the curve looks like a stack of single lines. The parameter box on left is to set the parameters of the burning process namely the ramping rate of the voltage up, the relative change in resistance at which the voltage is ramped down again, the rate with which the voltage is ramped down, the compliance level of the Keithley 2400 and the resistance goal of the tunneling junction. The algorithm which is embedded in this Labview program is shown in fig 4.8 in the

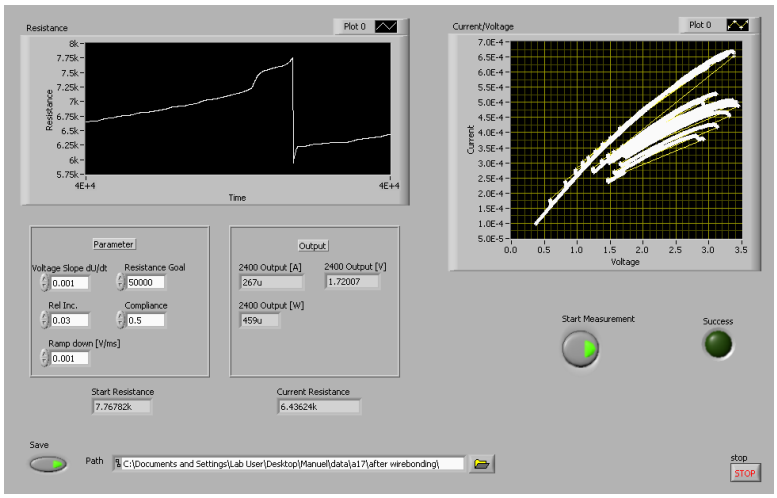

Figure 5.5: Front panel for the Labview Program which has been used for the gap formation.

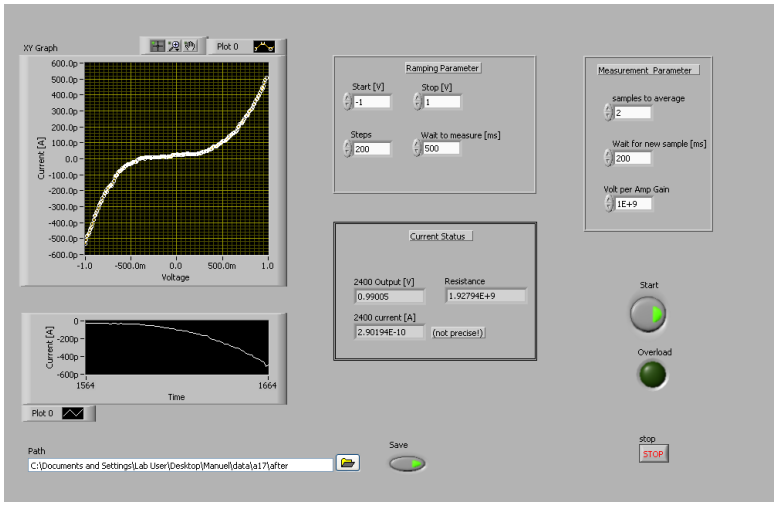

Figure 5.6: Frontpanel for the voltage/current measurements.

experiment chapter of this thesis.

Figure 5.6 shows the measurement of a tunneling curve. The large plot shows current on the Y-scale and voltage on the X-scale. The smaller plot below shows current through the sample as a function of time. This program has two boxes to set parameters. The first box in the middle upper section of the front panel sets the start and the stop voltage and the number of steps in between. If the resistance of a device is very high, the program increases the voltage and then waits for a few milliseconds for the capacitive currents to disappear. This parameter can be set in the "wait to measure" box. The second set of parameters in the upper right portion of the front

panel can be adjusted to increase the signal-to-noise ratio. One can choose how many samples with time delay at a certain voltage are measured and averaged. We usually took one to 5 samples with a time delay of about 1.5 times the rise time of the current amplifier. The last parameter is the gain set at the Keithley 427. Since the Keithley 427 has no digital interface, this value has to be copied by hand. The overload button indicates if the current through the current amplifier has exceeded its maximum value (10 Volts maximum output divided by the gain).

5.1.3 Development

We started with a very crude burning program which could set a voltage and measure resistance. We burned about a 50 graphene devices and 10 gold devices in total to optimize the burning program and the tunneling spectrum program. As the programs are written now they should be quite straightforward in use and quite user-friendly.

5.2 Equivalent circuit

To understand the electrical characteristics of the measurement system, it is useful to construct an equivalent circuit of the nanochannel device. The complete measurement setup is shown in chapter 4. The equivalent circuit is shown in fig. 5.7. $V_L(t)$ and $V_T(t)$ represent the voltage supply. $V_L(t)$ is applied on Ag/AgCl electrodes which contact the electrolyte, $V_T(t)$ is applied at the tunneling contacts. The measured currents are $I_T(t)$ and $I_L(t)$.

$X_T(t)$ is the transversal and $X_L(t)$ the longitudinal time dependent conductance. The tunneling information is embedded in $X_L(t)$. C_G is the capacitive coupling between the liquid and the leads through the silicon substrate. C_T is the capacitive coupling between the two tunneling electrodes. C_C is the conducting coupling between the conductive paths and the silicon bulk material of the chip. R_{Si} is the resistivity of the silicon chip and C_E the capacitive coupling between the silicon chip and the liquid. The equivalent circuit gives the following equations.

$$I_T(t) = \frac{V_T(t)}{X_T(t)} - C_G \frac{d(V_T(t) - V_L(t))}{dt} \tag{5.1}$$

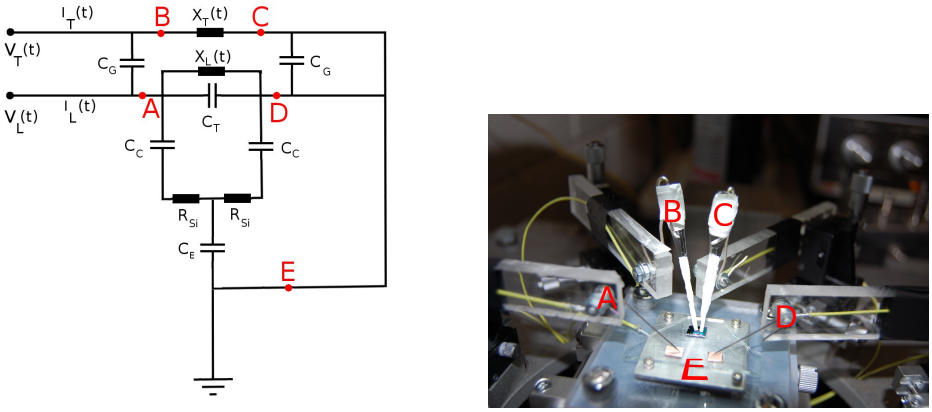

(a) (b)

Figure 5.7: Circuit of the embedded chip with power supplies. X_T is the transversal conductance through the nanochannel, X_L the longitudinal conductance. **a**, An equivalent circuit of the measurement setup which is necessary for future applications with high sampling rates. The points A, B, C, D and E are connections to a device. **b**, Picture of a contacted device. The points A, B, C, D and E are indicated.

$$I_L(t) = C_G \frac{d(V_T(t) - V_L(t))}{dt} + \frac{V_L(t)}{X_L(t)} + C_T \frac{dV_L(t)}{dt} + C_C \frac{dU_1}{dt} \tag{5.2}$$

$$0 = V_T(t) - U_1(t) - \frac{dU_1(t)}{dt} C_C R_{Si} - U_2 \tag{5.3}$$

$$0 = U_2 - \frac{dU_3}{dt} C_C R_{Si} - U_3 \tag{5.4}$$

$$\frac{dU_2}{dt} C_C = \frac{dU_1}{dt} C_E + \frac{dU_3}{dt} C_C \tag{5.5}$$

that can be solved numerically.

One can expect C_G to be quite small because the gold contacts and the liquid are far away from each other. C_T is also very small because it is just the capacity between two very small graphene tips. C_c can be quite important since the silicon substrate, accounted for with R_{Si} is a good conductor[3]. If we keep V_L and V_T constant, most of the circuitry does not contribute. $I_T(t)$ and $I_L(t)$ will only depend on the X_L and X_T.

[3]The Nova Wafer used have a specific resistance of $\rho = 10^{-3}\Omega m$.

Chapter 6

Methods

6.1 Imaging

A very important step in the fabrication of graphene devices is the ability to see it. We describe the three used methods here.

6.1.1 Optical

Graphene on top of a silicon oxide layer on silicon is visible if the silicon oxide has the correct thickness. The microscopy images presented here were taken with a Nikon Eclipse LV100 microscope. The machine is equipped with a pair of polarization filters that can be crossed to increase contrast of scattering sources. It is capable of differential interference contrast (DIC), an imaging mode similar to phase contrast to enhance the contrast of thin materials. It is also connected to a PC to save images.

6.1.2 TEM

Free standing graphene is visible in annular dark field (ADF). Graphene on amorphous materials is difficult to see in ADF mode because there is a lot of background. Diffraction patterns however can be easily identified.

We worked with suspended graphene on a catalog number 4230C, Quantifoil R1.2/1.3 $300\mu m$ C holey carbon grid and also with graphene on amorphous material, namely a Durasin Film DTF- 030523 from electron microscopy sciences. The maximum resolution of the JOEL2010F TEM/STEM microscope that we used is $0.2nm$.

6.1.3 SEM

We used a FEI Sirion Scanning Electron Microscope which can take images in TLD (Through lens detector) and SE (Secondary Electron) mode. The microscope is shown in fig. 6.4a. The maximum acceleration Voltage is 30keV. The maximum resolution that we can reach with this machine is about $10nm$. We pushed the limits of the electron microscope in the fig. 6.5. The SEM has also been used for lithography and the nanofabrication of the devices presented here. To control the beam the software $NPGS$[1] has been used together with a CAD drawing software.

The contrast of graphene on a silicon oxide surface is better at smaller acceleration voltages. Usually 5keV does a good job [38]. The disadvantage of the small acceleration voltages is that the brightness is not very high from the lack of secondary electrons. We tried to image graphene with small acceleration voltages as far as possible.

6.2 Graphene production

6.2.1 Chip preparation

The fist step to prepare a new device is the selection of a suited substrate. We use silicon wafers from "Nova Electronic Materials" with a $\langle 100 \rangle$ surface, covered with $300nm$ of chlorinated and thermally grown oxide. The wafer is boron doped with a conductivity of $10^{-3}\Omega m$. To prepare a new sample, a piece of the wafer is cut with a diamond cutter and cleaned from a protecting PMMA film with sonication for 10min in Acetone[2] followed by rinsing in Isopropyl alcohol[3]. The bare samples can be stored in a dry place.

---

[1] Nanometer Pattern Generation System by JC Nabity Lithography Systems.

[2] Acetone is supplied by Fisher Sci. It fits ACS specification and is spectral analyzed.

[3] Also by Fisher Sci.

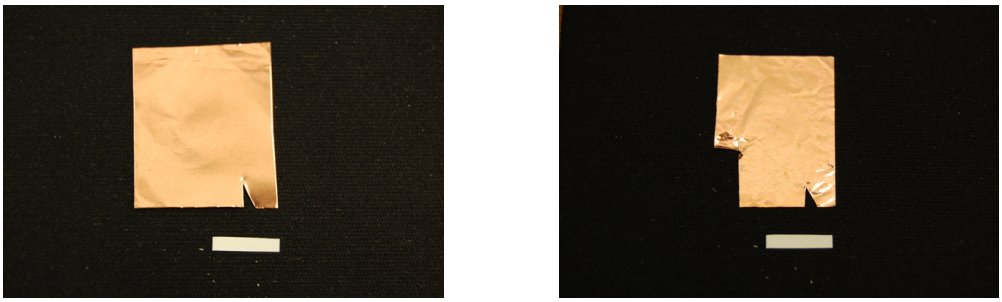

(a) (b)

Figure 6.1: A piece of Copper before growth and after. The scale bar in both pictures is 1cm. **a**, A piece of copper foil of a typical size before graphene growth. **b**, The same piece of copper after the growth. A small piece of the foil has been removed for a transfer to silicon.

6.2.2 CVD growth

All CVD growth was performed on copper foil[4]. We followed a recipe described by Li et al. [65]. Graphene growth on Nickel is also quite popular and has the advantage of more uniform layers. A piece of copper before and after the growth is shown in fig. 6.1. Small pieces on the left side have been removed to transfer the graphene to a substrate. The transfer technique is described in detail in fig. 6.3.

The recipe of growing graphene on copper is as follows:

- Place a piece of copper, size approx. 2cmx3cm on a piece of quartz and place it in a furnace[5]. A sample piece is shown in fig. 6.1a. A picture of the tube furnace used throughout this thesis is seen in fig. 6.2a.
- Let approximately 2000sccm of forming gas, a mixture of 10%H_2 and 90% Ar, flow over the copper[6] and heat the furnace to 1050°C.
- Wait for 2h to 3h for the copper to anneal and the surface to be cleaned. The hydrogen will reduce all copper oxides on the surface and the high temperature will increase the grainsize of the copper.

[4]Basic Copper, Carbondale, IL with a purity of 99.9% and a thickness of 25μm.

[5]The Furnace we used is a Applied Test Systems Inc. Series 32100 Split tube Furnace.

[6]We used a gas mixture supplied by GTS Welco.

- Add 40sccm of 1% CH_4 and 99% Ar to the gas flow[7]. The methane concentration is 200ppm[8]. The graphene growth starts as soon as methane is added to the forming gas. Typical growth times are 10min-30min. The results are shown in the beginning of the experiments chapter in fig. 4.1.

- Close the walve for the methane mixture when the graphene growth shall be stopped.

- Switch off the furnace and let the sample cool down under a continuous flow of 10%H_2 and 90% Ar.

- To cool the sample faster, the quartz tube with the sample in it can be removed from the furnace as soon as the temperature falls below 600°C

The result is a piece of copper foil with graphene on top. It is shown in fig. 6.1b. To transfer the graphene to a Silicon/Siliconoxide wafer another step is needed.

- Spincoat the upper side (the side with the graphene on it) of the copper foil with PMMA, A6[9] for 1min at 2000rpm.

- Bake the PMMA at 180°C for 5min on a hotplate.

- Place the foil with the lower (not PMMA covered) side up in a reactive ion etcher (RIE)[10]. Expose the sample to oxygen plasma for 1min at 50W output and a pressure of 50mTorr. The Oxygen plasma will remove the carbon material from the surface so that only the layer of graphene, protected by PMMA remains. The RIE machine is shown in fig. 6.2b.

- Remove copperfoil from the RIE.

---

[7] Also a mixture from GTS Welco. However their error bar indicates $1 \pm 1\%$ methane.

[8] 200 parts per million because $40 \cdot 0.01/2000 = 0.0002$.

[9] 6% of 950 Poly(methyl methacrylate) diluted in Anisole.

[10] We used Reactive Ion Etcher, Torr International Inc., model RIE300W-3MFC.

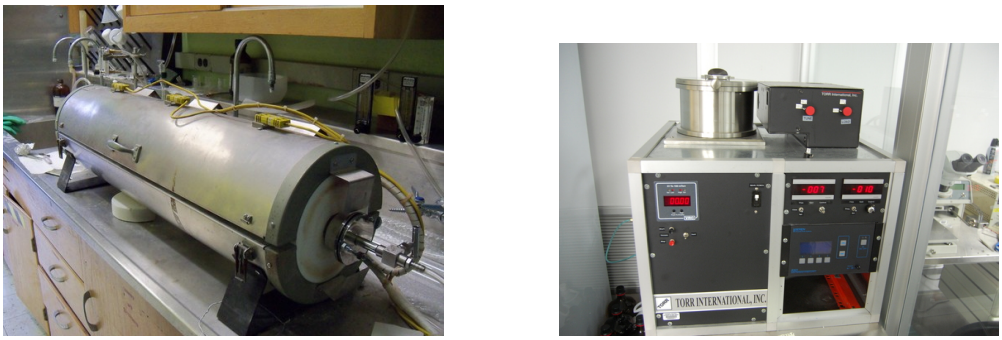

(a) (b)

Figure 6.2: **a**, Furnace used for the CVD growth of graphene. **b**, Reactive Ion Etcher (RIE) used to etch patterns in graphene.

After the two steps above the graphene on copper is ready for transfer to a new substrate. The copper foil can also be stored in a dry place for future use. We used copper foil with CVD graphene on it in a timescale of several weeks.

The transfer process from the copper foil to a piece of wafer is as follows:

- Cut a small piece of the copper foil with PMMA and graphene on top with a pair of scissors. The size should be around $3mm \times 3mm$. Place this piece, glued with tape[11] in a petri dish.

- Fill the petri dish with a 22.3% (by weight) $FeCl_3$ solution[12]. The ferric chloride solution will etch the copper so that a free floating PMMA film with graphene below remains. The etching process takes about 2 to 3 hours (we usually do it over night).

- Rinse the floating PMMA pieces taped to the bottom of the dish several times with $\approx 10\%$ hydrochloric acid[13] and water to remove all remaining $FeCl_3$.

- Let the PMMA films float on the surface of water and place a cleaned chip underneath it (in the water). Remove the water with a pipette and the films will sit atop of the chips.

[11] Ultron Systems Inc. Adhesive Plastic Film 1007R, We have a few sample sheets.

[12] $FeCl_3$ in Lumps is from Fisher Scientific. It fits ACS specifications and is diluted in water.

[13] Coreo Chemical Coperation Reagent Grade $> 36.5\%$ 11.25ml in 88.75ml water.

- Dry the films on a hotplate at $\approx 180°C$ for 30min.
- Remove the PMMA with hot acetone.

The graphene on the silicon oxide film can now be imaged with optical microscopy or the microscopy method of choice. A few examples are shown in the beginning of the experiments section in fig. 4.1.
The transfer of graphene onto a TEM grid works different. We follow the recipe by Regan et al. [97].

- Cut a small piece of copper foil with graphene grown on it but which is not covered with PMMA.
- Place the TEM grid face down onto the graphene side of the copper foil. It is convenient to do everything in a Petri dish.
- Place a drop of Isopropyl alcohol onto the TEM grid and let it dry. The drying process will make a good connection between the graphene and the TEM grid. After the drop dried the stack can be placed on a hotplate at $\approx 100°C$ for 5 minutes.
- Let the Copper foil/TEM-Grid stack float on top of a ferric chloride solution[14] which is filled into the Petri dish. It will etch the copper so that the graphene now sticks to the TEM grid.
- Clean the TEM grid by hydrochloric acid and distilled water. Silicon nitride grids can also be cleaned in the furnace.

6.3 Device Fabrication

To fabricate a device the first step is growing graphene and transferring the graphene to a Silicon/Silicon dioxide chip. The next step is e-beam lithography to build a PMMA structure on the chip. The last step is a metal deposition to build the structure from Au/Ti.

[14] Again 22.5% by weight.

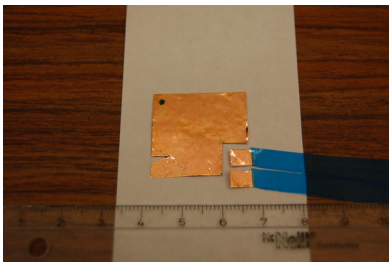

(a) Cut a piece of copper with graphene on it.

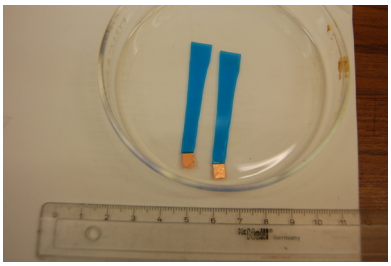

(b) Tape it into a Petri dish.

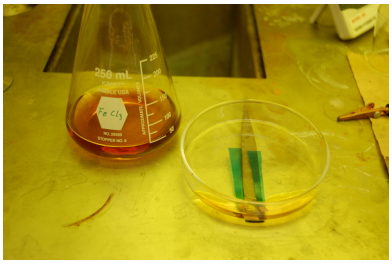

(c) Let it float on $FeCl_3$ solution.

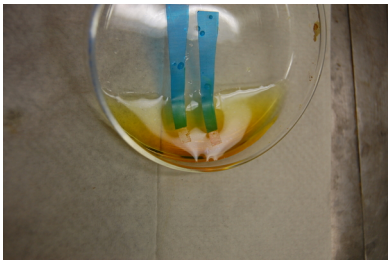

(d) until the copper foil is etched.

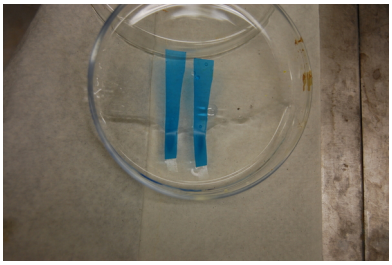

(e) Rinse in water/HCl

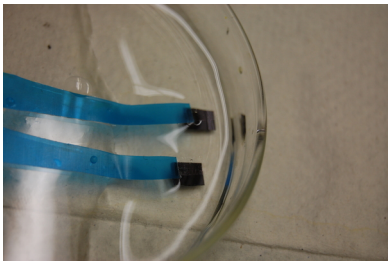

(f) And place a chip underneath.

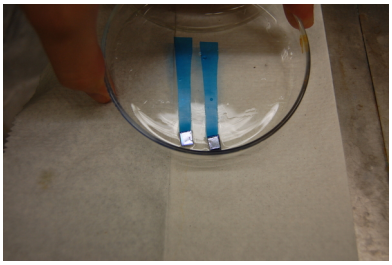

(g) Remove the water with a pipette.

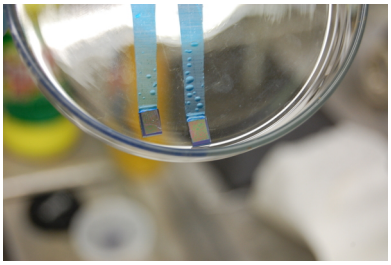

(h) And dry the sample on a hotplate.

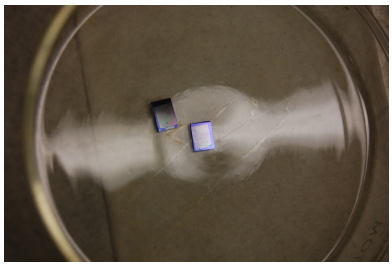

(i) Remove Tape

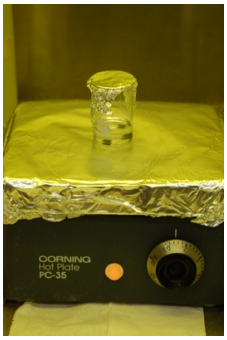

(j) And the PMMA in hot acetone.

Figure 6.3: The complete CVD graphene transfer process in detail.

(a) (b)

Figure 6.4: **a**, The FEI Sirion SEM in lithography mode. **b**, The metal evaporation chamber.

6.3.1 E-beam lithography

To produce patterns on a chip we use electron beam lithography. PMMA is a non toxic polymer which, once exposed to a certain radiation dose, changes its molecular structure so that it becomes solutable in certain solvants.

- Spincoat the sample with EL3, 4000rpm for 1min and dry for 1:30min at 180°C.
- Spincoat another layer of A6, 4000rpm for 1min and dry for 1:30min at 180°C.
- Place the sample in the SEM.
- Pump SEM chamber und correct for astigmatism and focus. Find the spot to do lithography with.
- Switch to the NPGS system, use its imaging mode to align the sample. Fig. 6.4a shows the SEM in lithography mode.
- Draw the patterns, prepared with the CAD program of choice, with an area dose of 520$\mu C/cm^2$ and a line dose of 25nC/cm.
- Remove the sample from the SEM.

Other line and area doses can also be used. In the next section we will push the resolution limits of the e-beam system. We will use PMMA-950 2% in anisole and a very small line dose.

6.3.2 Metal deposition and Contacting

If the structure has been build into the PMMA the next step is the removal of exposed PMMA and the deposition of metal.

- After the lithography, expose the sample for 1min to Methyl isobutyl ketone (MIBK) : Isopropanole (1:3) to remove exposed PMMA[15].
- Rinse the sample in isopropanole and blow it dry with a nitrogen gun.
- Place the sample in a metal evaporation chamber[16]. The machine is shown in fig. 6.4b.
- Deposit 3nm of titanium as a glue.
- Deposit 50nm of gold.
- Remove the sample from the evaporation chamber and lift off the PMMA with hot acetone.
- The lift-off usually takes an hour. After that rinse the sample in isopropanole.

Thinner layers of gold do not require any glue. We have used a very thin gold layer to draw very small structures.

6.3.3 Limits of e-beam lithography

For the nanochannel purposes it is interesting to make structures as small as possible. Experiments with test-patterns as in fig. 6.5 reveal, that the resolution is about 50nm or so which is quite close to the imaging resolution limit.

The test patterns shown in fig. 6.5 are drawn in A2 PMMA, spincoated with 4000rpm for 40sec and dried at $150°C$ for 1'30". The exposure of the line is 15 nC/cm and 7nm gold have been deposited. Thin films do not need a binding layer of titanium to stick to a surface. To assist the lift-off, which is extremely difficult with thin films,

[15]The developer is a commercial product MIBK/IPA 1:3 Developer from Micro Chem.

[16]We used a machine with an e-beam evaporation source in a UHV two chamber system.

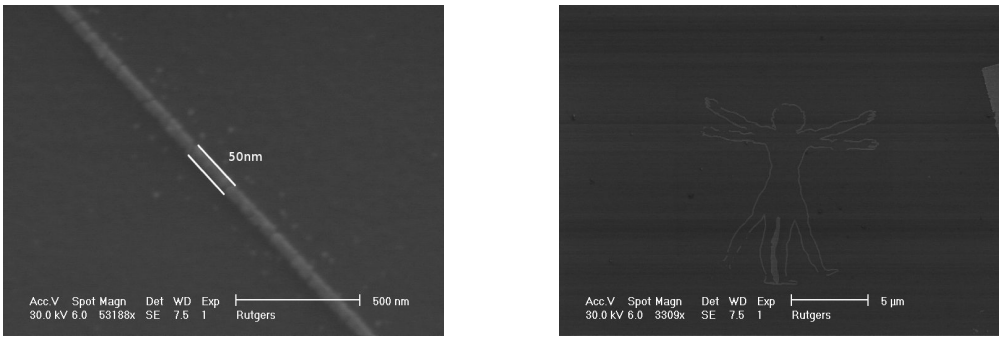

(a) (b)

Figure 6.5: Test-patterns to measure the smallest structures which we can build with our setup to do e-beam lithography. **a**, The resolution limit of lithography. The line is about 50nm in width and 7nm of height. The material is gold. **b**, Da Vinci's *Vitruvian Man* from a very thin line.

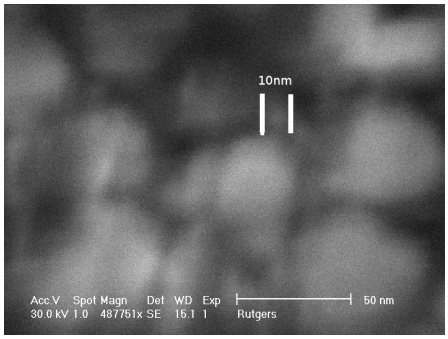

Figure 6.6: The SEM resolution limit is about 10nm as can be seen here. The resolution limit together with the poor contrast is the main problem of imaging graphene nanostructures.

about 3% Triton-X[17] have been added to the hot acetone. It is supposed to minimize the effect that loose gold particles from the lift-off stick to the surface. As a detergent it acts like a soap and covers the floating gold with a micelle-like cover.

The smallest structures in the imaging mode that can be resolved are of the size of $\approx 10nm$. A picture of some gold nanoparticles is shown in fig. 6.6.

6.3.4 Etching Recipes

Etching silicon dioxide is usually done with hydrofluoric acid. Since HF is quite toxic it is usually buffered in Ammonium fluoride solution. To etch silicon oxide the sample

[17] Alfa Aesar, A16046

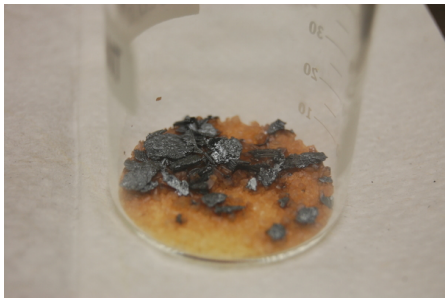

Figure 6.7: Preparation of the gold etchant. The white crystals are potassium iodide and the black flakes are crystals of elemental iodine.

is placed in this buffer etch[18].

Gold etching is done with potassium iodide and elemental iodine[19] solved in water.

The recipe of the cold etch used is as follows:

- 4g of potassium iodide, 1g of iodine in 20ml of water.
- Place the sample in the etching solution for the required time. The nanochannel devices have been etched for about 24h.
- Gold gets removed by the reaction to gold iodide ($2Au+J_2 \rightarrow 2AuJ$).
- When the samples has finished etching, it is rinsed in water and isopropanol.

6.3.5 Nanochannel fabrication

The nanochannels used in this thesis are made by e-beam lithography. The production method is as follows:

- Start with a graphene device on a thermal oxide covered wafer.
- Spincoat A6/EL3 as described in the lithography section and draw the nanochannel pattern.
- Develop pattern, deposit Gold by metal evaporation (As we explained, no Titanium glue is required for very thin layers).

[18]Commercial product J. T. Baker 10:1.

[19]KJ from Fisher Scientific, USP. Elemental iodine supplied by Cerac Speciality Inorganics, at least 99.999%

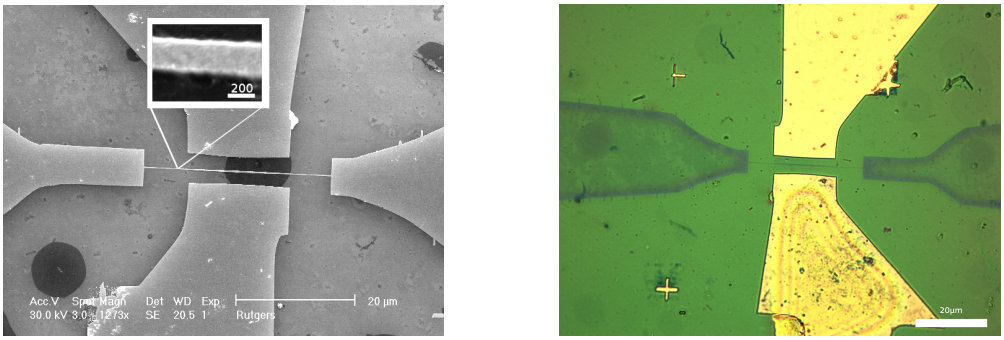

(a) (b)

Figure 6.8: Two main steps on the way to a nanochannel device. **a**, The nanochannel sacrificial layer structure across a graphene hexagon in SEM. **b**, Successful sacrificial layer etching to form a nanochannel across the hexagon. This picture is optical. The nanochannel here is covered with $\approx 120nm$ of Al_2O_3. Later we switched to a 300nm thick layer of Al_2O_3 for more stability.

- Lift-off with hot acetone and a few percent Triton-X.
- Protect the future opening of the nanochannel structure and of the metal contacts with a piece of tape.
- Sputter the entire surface with alumina. We RF sputtered off an aluminum oxide target in argon plasma at $5 \cdot 10^{-3} torr$ and 100W. The sputtering rate is $\approx 5 \frac{nm}{min}$. We sputtered for 60min to create an $\approx 300nm$ thick film of Al_2O_3.
- Remove the tape on the tunneling leads and spincoat a thick layer of PMMA on top.
- Now remove the tape from the nanofluidic entries: The gold lies bare to the surface whereas the tunneling leads are protected by PMMA.
- Etch gold with the gold etch. The recipe is given above.
- Check nanochannel by longitudinal conductance measurements with two Ag/AgCl electrodes.

The process of continuous etching is shown in fig. 6.9. The 7nm gold layer which appears as red is covered with PMMA except at the rectangular spot. A microscope picture is shown in Fig. 6.9a. The gold is etched with gold etch as it can be seen in fig.

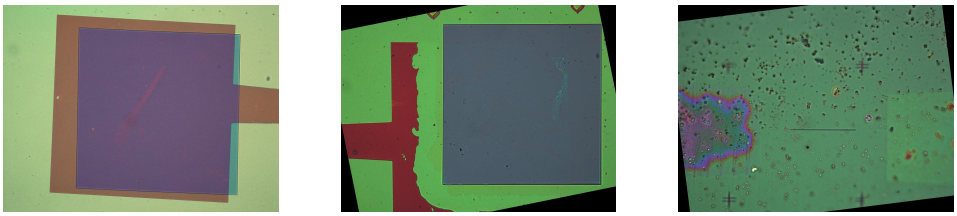

(a) (b) (c)

Figure 6.9: Nanochannel fabrication; the microscopic process of removing gold. **a**, Gold is buried under PMMA and a window to the gold has been opened. The 7nm thin gold film appears red. **b**, The gold etching has started. **c**, A very small line of gold is still remaining in the constriction of a nanochannel. The constriction is about $100nm$ in width and $7nm$ in height.

6.9b. In fig. 6.9c a small strip of gold remained in the nanochannel. This particular nanochannel has been used to show the effect of gold blocking a nanochannel in the experimental section in fig. 4.17a.

6.4 Device Measurement

6.4.1 Contacting a device

If the sample is to be measured in the probe station it can be contacted directly by stainless steel tips on the the gold leads. It can also be wirebonded to an external metal structure which can be contacted by the needles. This can be seen in fig. 6.11a. If it is to be measured in vacuum it is in every case to be wirebonded. The chamber used to measure a device in vacuum and different atmospheres is shown in fig. 6.12a. A wirebonded sample in the vacuum chamber is shown in fig. 6.12b. The process of measuring a sample is as follows:

- After the lift-off the sample is to be cleaned in forming gas for 5h at $230°C$.
- Then the sample is glued to a sample holder (with rubber cement or silver glue).
- Aluminum/Silicon wire is used to wirebond the gold contacts on the chip with contacts on the sample holder.

The other way is using the needle contacts of the probe station right on the sample. Then the process is as follows:

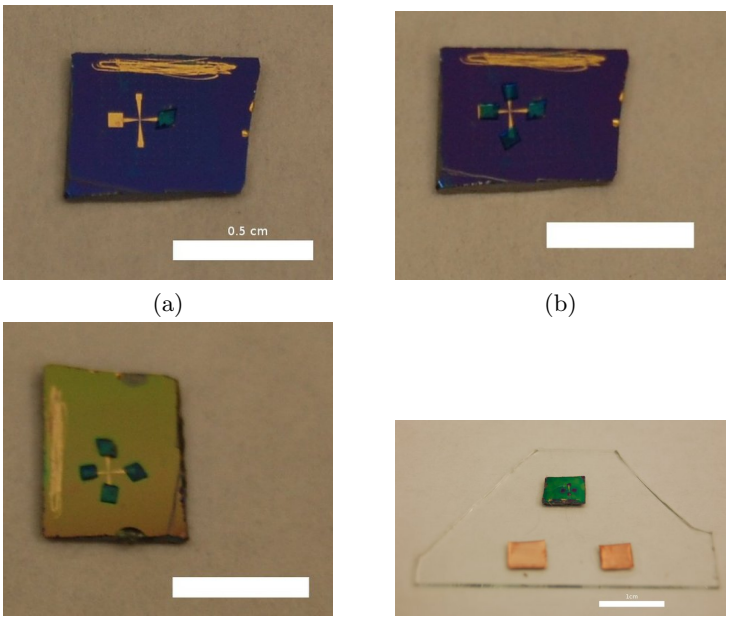

(a) (b)

(c) (d)

Figure 6.10: Fabrication of a nanochannel device macroscopically. **a**, Device with tape on access ports. Inset is 0.5cm. **b**, Tape on all future access points. Inset is 0.5cm. **c**, Nanochannel with alumina sputtered on top. The inset is 0.5cm. The color has changed due to an interference effect: the aluminum oxide sputtered surface is thicker than the pure silicon oxide layer in fig. 6.10c. **d**, Contacted nanochannel device. The tunneling electrodes are wirebonded to the copper contacts which can be contacted with the probestation without risking to destroy the device. The inset is 1cm.

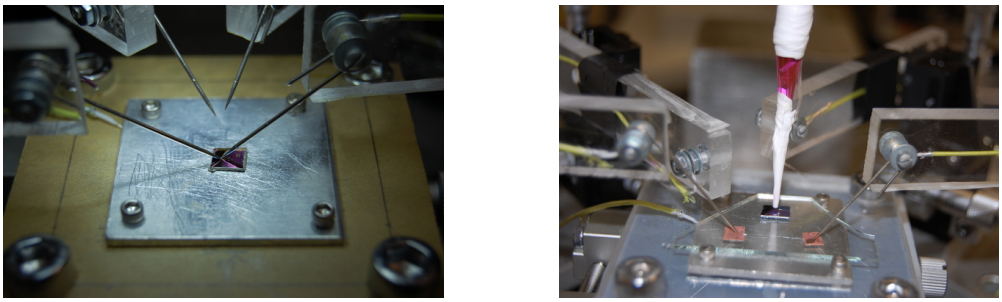

(a) (b)

Figure 6.11: The contacting of a device in the probestation as it is done with the nanofluidic devices. **a**, A nanofluidic device contacted in the probestation. **b**, A Wire-bonded and contacted device in the probestation. Also visible is the liquid contact filled with a Rhodamine B solution.

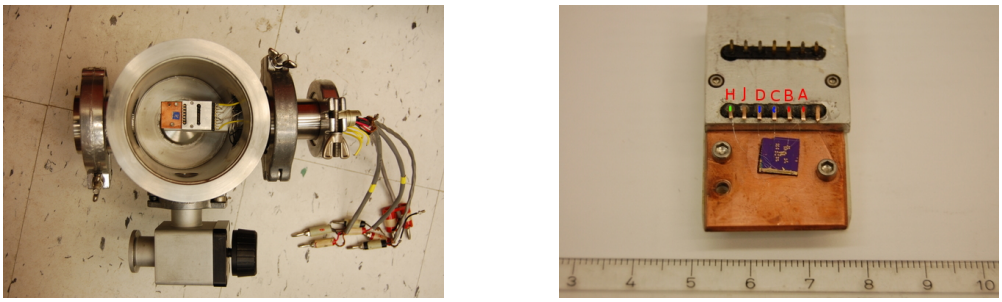

(a) (b)

Figure 6.12: Contacting a device in the vacuum/gas chamber. **a**, The entire vacuum/gas chamber. **b**, The sample holder of the chamber. 6 contacts are accessible, indicated as A, B, C, D, J and H. We used A and B for one device (red), C and D for another device (blue). J has not been used and H is connected to the gate (green).

- After the lift-off the sample is to be cleaned in forming gas for 5h at 230°C.
- Place the sample in the probe station, touch the gold contact plates with stainless steel needles.

6.4.2 Measurements with Electrodes

If measurements are to be performed with an electrode contacting a liquid, Ag/AgCl is the electrode material of choice. To make liquid contacts we used glass pipettes sealed with Teflon tape[20] and a tiny opening. The process is as follows:

[20] TaegaSeal PTFE Tape, Commercial Grade.

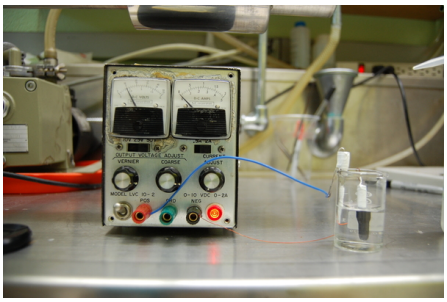

(a)

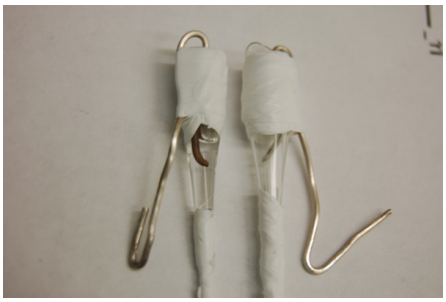

(b)

Figure 6.13: Shown is the setup to cover silver electrodes electrolytically with silver chloride and the result. **a**, The setup for the electrolytic AgCl deposition. The silver electrode is placed in a beaker together with a graphite electrode. **b**, Covered liquid electrode and another electrode for comparison. The silver chloride appears blackish because it is photosensitive.

- Cut off a Pasteur pipette the constriction in the front and the elongated tail. We get the two pieces shown in fig. 6.14a
- Cut from the thin front part a short piece. Roll some Teflon tape around the middle spot. It looks like fig. 6.14b.
- Place the glass/Teflon piece in the constricting part of the pipette and seal it with teflon tape. It is shown in fig 6.14c and fig 6.14d.
- Place a piece of silver wire in the electrode, seal it with Teflon tape. It is shown in fig. 6.14e and 6.14f.
- Cover the open bottom side of the pipette with Teflon tape and punch a tiny hole into the tape using sharp tweezers.

The next step is the deposition of silver chloride on the electrode.

- Attach a piece of silver wire[21] within the electrode to the positive pole and a piece of graphite as negative pole of a power supply in 10% hydrochloric acid[22].
- Electrolyse at 5V. The current is quite small.

[21] Alfa Aesar Silver Wire, 1.0mm dia, hard, 99.9%.

[22] Coreo Chemical Coperation Reagent Grade > 36.5% 11.25ml in 88.75ml water.

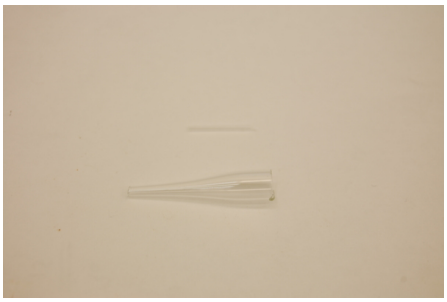

(a) Two parts of a Pasteur pipette.

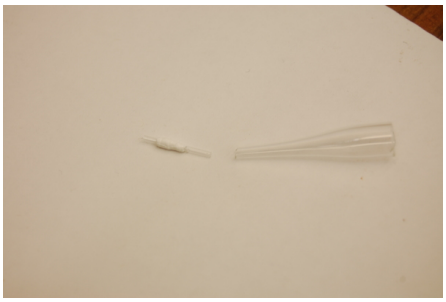

(b) Wrap Teflon tape around the small piece

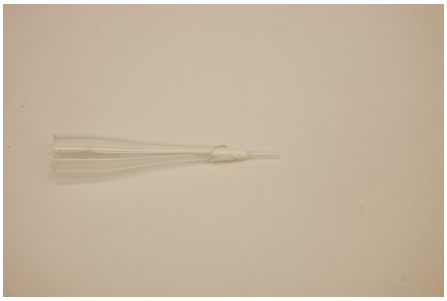

(c) Place it in the larger piece

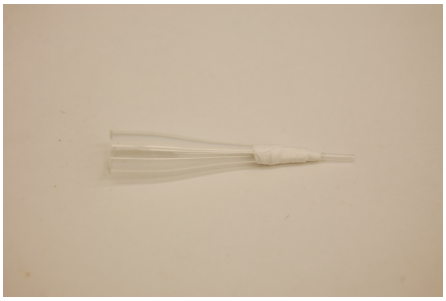

(d) Wrap it with Teflon tape.

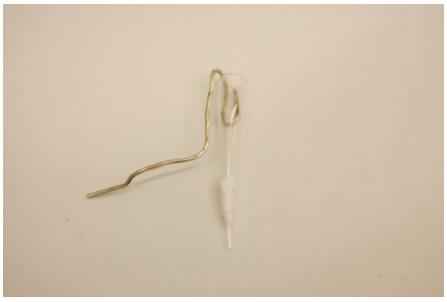

(e) Add a piece of silver wire

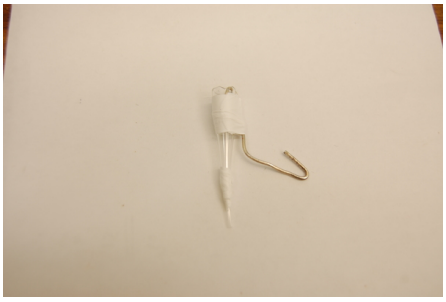

(f) And wrap it as well.

Figure 6.14: Fabrication of the liquid electrode contacts.

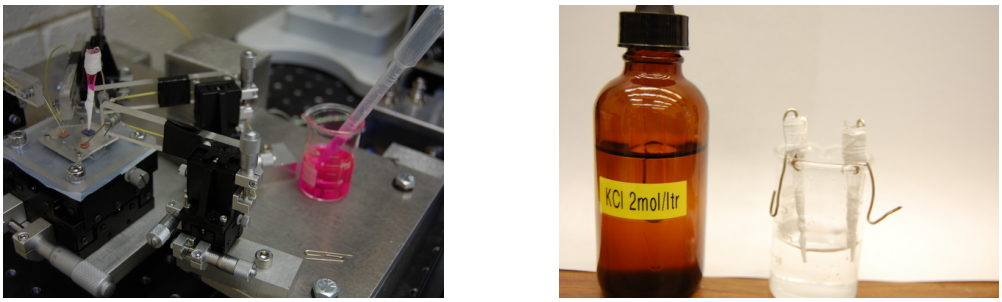

(a) (b)

Figure 6.15: Two electrodes in use and in storage. **a**, Nanochannel and Rhodamine B solution. **b**, Storage of the Ag/AgCl electrodes.

- Electrolyse until the silver gets covered with a white substance. Usually it takes $\approx 1min$. The color will later change because silver chloride is photosensitive. The silver ions become elemental silver again and the color of the electrode changes to dark brown.

Store the electrode in KCl solution[23]. If the electrode has not been used for a while, dry it, polish it, clean it with acetone and isopropanole and deposit a new layer of AgCl with the method atop.

The liquid contacts can be filled from the backside with the solution of one's choice. An example is shown in fig. 6.15a. The electrodes are filled with a Rhodamine B solution.

[23]KCl from Carolina Biological Supply Company. Fulfilling ACS regulations.

Appendix A

A model for noise in the tunneling junction

A.1 Tunneling through DNA

A molecule between two conductors is a tunneling device. If the Hamiltonian H and overlap matrices S of the electrode-DNA-electrode systeme are known, one can immediately write down the Green's function of the electrode-DNA-electrode system [52] [102] [136]

$$G(E) = \frac{1}{ES - H - \Sigma_1 - \Sigma_2} \tag{A.1}$$

Σ_1 and Σ_2 are the self-energy terms due to the electronic structure of the two electrodes. Measuring different nucleobases means a change in the Hamiltonian itself caused by the different energy levels of the molecular orbitals and a change in the overlap of the electrode and the molecule orbitals due to the relative change in size. The transmission coefficient is [1]

$$T(E) = Tr(\Gamma_1 G \Gamma_2 G^\dagger) \tag{A.2}$$

where $\Gamma_{1(2)} = i(\Sigma_{1(2)} - \Sigma^\dagger_{1(2)})$ [2]. The current between the two electrodes, assuming an uniform density of states within the electrodes, is then given [3] by

$$I = \frac{2e}{h} \int_{-\infty}^{\infty} dE T(E)(f_1(E) - f_2(E)) \tag{A.3}$$

where $f_{1(2)} = (\exp(\beta(e - \mu_{1(2)})) + 1)^{-1}$ is the Fermi function and $\mu_{1(2)}$ the chemical potential of the two electrodes.

---

[1] From [16] and also Eqn (3.224) in [18].

[2] Eqn (3.225) in [18].

[3] Eqn (3.229) in [18]

A.2 A model for noise in the DNA/Electrode system

One can use a simplified picture of the system with only one single energy level E_0 in the junction. We can choose this energy level to be HOMO or LUMO. It may interact with its environment with the model Hamiltonian [43] [52]

$$H = E_0 d^\dagger d + H_{de} + H_e + d^\dagger d \sum_k g_k \left(b_k^\dagger + b_k\right) + \sum_k \omega_k b_k^\dagger b \tag{A.4}$$

$E_0 d^\dagger d$ accounts for the electrons within the LUMO, H_{de} is the DNA-electrode interaction, H_e the electrodes' Hamiltonian itself. $\sum_k \omega_k b_k^\dagger b$ represents a bosonic environment which interacts with the electrons in the molecule via $d^\dagger d \sum_k g_k \left(b_k^\dagger + b_k\right)$. In [43] this Hamiltonian is used to modell an electron/phonon interaction in a resonant tunneling device. However it is also applicable to the electrode-DNA-electrode system with environmental interaction as a source of noise. The Green's function for this Hamiltonian can be written as[4]

$$G(t) = -i\Theta(t) e^{-i\tilde{E}_0} e^{-\gamma t} e^{-\phi(t)} \tag{A.5}$$

$\tilde{E}_0$ is the renormalized energy level, γ the coupling strength to both electrodes and $e^{-\phi(t)}$ accounts for the coupling to the environment. The bosonic term is[5]

$$\phi(t) = \sum_k \frac{|g_k|^2}{\omega_k^2} \left(n_k \left(1 - e^{i\omega_k t}\right) + (n_k + 1)\left(1 - e^{-i\omega_k t}\right)\right) \tag{A.6}$$

where $n_k = (\exp(\beta\omega_k) - 1)^{-1}$ is the Bose distribution of the mode k. For a temperature larger then the boson cutoff at a certain fequency ω_c, $n_k + 1 \approx n_k$ and therefore

$$\phi(t) = \sum_k \frac{2|g_k|^2}{\beta\omega_k^3}(1 - \cos(\omega t)) \tag{A.7}$$

ϕ and $\tilde{E}_o$ can also be expressed in terms of the spectral function $J(\omega) = \sum_k |g_k|^2 \delta(\omega - \omega_k)$ and holds

$$\phi \approx \int_0^{\omega_c} \frac{2J(\omega)}{\beta\omega^3}(1 - \cos(\omega t)) d\omega \tag{A.8}$$

$$\tilde{E}_0 = E_0 + \int_0^{\omega_c} \frac{J(\omega)}{\omega} d\omega \tag{A.9}$$

[4] Eqn. (66) in [43].

[5] Eqn. (68) in [43] and Eqn. (10) in [52].

The spectral function for an ohmic boson bath is linear $J(\omega) = \alpha\omega$ for $\omega < \omega_c$ [29]. Now both integrals can be calculated $\phi \approx \frac{\alpha\pi}{\beta}t$ and $\tilde{E}_0 = E_0 + \alpha\omega_c \approx E_0$ for ω_c large enough to perform the ϕ integration and small compared to the molecular energy levels E_0. This gives eventually the retarded Green's function of the electrode-DNA-electrode system with a bosonic source of noise

$$G(E) = \frac{1}{E - E_0 + i\gamma + i\eta} \tag{A.10}$$

where $\eta = \alpha\pi/\beta$. The current can be calculated from the Green's function [18].

$$I(\eta) = \frac{2e^2V}{h}\left(\frac{\gamma^2}{E_0^2 + (\gamma+\eta)^2} + \frac{\eta\gamma}{E_0^2 + (\gamma+\eta)^2}\right) \tag{A.11}$$

η ist the bosonic noise term with the unit [energy]. It is therefore the inverse of a certain timescale at which energy exchange can take place. As expected an increase in noise will decrease the current through the tunnel junction. If we allow γ (the coupling to the electrodes) to follow a gaussian distribution due to the non-static position of the nucleobase in the junction [52]

$$p(\log(\gamma/\gamma_m)) = \frac{1}{\sqrt{2\pi\sigma_\gamma^2}} e^{-\frac{1}{2}\left(\frac{\log(\gamma/\gamma_m)}{\sigma_\gamma}\right)^2} \tag{A.12}$$

we will measure a distribution of currents, broadened by γ and η.

References

[1] M. Akeson, D. Branton, J. J. Kasianowicz, E. Brandin and D. W. Deamer: *"Microsecond time-scale discrimination among polycytidylic acid, polyadenylic acid and polyuridylic acid as homopolymers or as segments within single RNA molecules"*, Biophys. J. 77(6): 3227-3233 (1999)

[2] S. Alwarappan, R. K. Joshi, M. K. Ram and A. Kumar: *"Electron transfer mechanism of cytochrome c at graphene electrode"*, Appl. Phys. Lett. 96(26): 3702 (2010)

[3] Y. Astier, O. Braha and H. Bayley: *"Toward single molecule DNA sequencing: Direct identification of ribonucleoside and desoxyribonucleoside 5'-monophosphates by using an engineered protein nanopore equipped with a molecular adapter"*, J. Am. Chem. Soc. 128(5): 1705-1710 (2006)

[4] O. T. Avery, C. M. MacLeod and M. McCarty: *"Studies on the chemical nature of the substance inducing transformation of pneumococcal types. Inductions of transformation by a desoxyribonucleic acid fraction isolated from pneumococcus type III"*, J. Exp. Med. 79(2): 137-158 (1944)

[5] V. S. Bagotsky: *"Fundamentals of Electrochemistry"*, Wiley-Interscience, 2 edition (November 25, 2005)

[6] J. B. Bates, Y. T. Chu and W. T. Stribling: *"Surface topography and impedance of metal-electrolyte interfaces"*, Phys. Rev. Lett. 60(7): 627-630 (1988)

[7] D. Branton et al.: *"The potential and challenges of nanopore sequencing"*, Nature Biotech. 26: 1146-1153 (2008)

[8] R. W. de Boer and A. van Oosterom: *"Electrical properties of platinum electrodes: Impedance measurements and time-domain analysis"*, Med. Bio. Engin. Comp. 16(1): 1-10 (1976)

[9] T. Z. Butler, J. H. Gundlach and M. A. Troll: *"Determination of RNA orientation during translocation through a biological nanopore"*, Biophys. J. 90(1): 190-199 (2006)

[10] H. Chang et al.: *"DNA-mediated fluctuations in ionic current through silicon oxide nanopore channels"*, Nano Lett. 4(8): 1551-1556 (2004)

[11] F. Chen and N. J. Tao: *"Electron Transport in Single Molecules: From Benzene to Graphene"*, Acc. Chem. Res. 42(3): 429-438 (2009)

[12] P. Chen et al.: *"Probing single DNA molecule transport using fabricated nanopores"*, Nano Lett. 4(11): 2293-2298 (2004)

[13] N. G. Cooper: *"The Human Genome Project: deciphering the blueprint of heredity"*, University Science Books; Revised edition (March 1994)

[14] F. H. Crick, L. Barnett, S. Brenner and R. J. Watts-Tobin: *"General nature of the genetic code for proteins"*, Nature 192: 1227-1232 (1961)

[15] R. Dahm: *"Discovering DNA: Friedrich Miescher and the early years of nucleic acid research"*, Hum. Genet. 122(6): 565581 (2008)

[16] S. Datta: *"Electronic Transport in Mesoscopic Systems"*, Cambridge University Press: Cambridge (1995)

[17] S. Datta et al.: *"Current-Voltage Characteristics of Self-Assembled Monolayers by Scanning Tunneling Microscopy"*, Phys. Rev. Lett. 79(13): 2530-2533 (1997)

[18] M. Di Ventra: *"Electrical Transport in nanoscale Systems"*, Cambridge University Press; Cambridge (1998)

[19] J. C. T. Eijkel, J. Bomerand, N. R. Tas and A. van den Berg: *"1-D Nanochannels fabricated in polyimide"*, Lab Chip 4(3): 161-163 (2004)

[20] A. A. M. Farag and I. S. Yahia: *"Structural, absorption and optical dispersion characteristics of rhodamine B thin films prepared by drop casting technique"*, Optics Comm. 283(21): 4310-4317 (2010)

[21] A. C. Ferrari: *"Raman spectroscopy of graphene and graphite: Disorder, electron-phonon coupling, doping and nonadiabatic effects"*, Sol. State Comm. 143: 47-57 (2007)

[22] A. C. Ferrari and J. Robertson: *"Interpretation of Raman spectra of disordered and amorphous carbon"*, Phys. Rev. B 61(20): 14095-14107 (2000)

[23] M. D. Fischbein and M. Drndi: *"Sub-10nm Device Fabrication in a Transmission Electron Microscope"*, Nano Lett. 7(5): 1329-1337 (2007)

[24] D. Fologea et al.: *"Detecting Single Stranded DNA with a Solid State Nanopore"*, Nano Lett. 5(10): 1905-1909 (2010)

[25] D. Fologea, J. Uplinger, B. Thomas, D. S. McNabb and J. Li: *"Slowing DNA translocation in a solid-state-nanopore"*, Nano Lett. 5(9): 1734-1737 (2005)

[26] M. Fouad and M. Yavuz: *"Nanofluidic channels fabricated by e-beam lithography and polymer reflow sealing"*, Vac. Sci. Technol. B 28(6): C6I11 - C6I13 (2010)

[27] H. Fricke: *"The theory of electrolytic polarization."*, Philosphical Magazine 14(90): 310-318 (1932)

[28] Garaj S. et al.: *"Graphene: A sub-nanometer trans-electrode membrane"*, Nature 467: 190-193 (2010)

[29] A. Garg, J. N. Onuchic and V. Ambegaokar: *"Effect of friction on electron transfer in biomolecules"*, J. Chem. Phys. 83(9): 4491-4503 (1985)

[30] D. Graf et al.: *"Spatially Resolved Raman Spectroscopy of Single- and Few-Layer Graphene"*, Nano Lett. 7(2): 238-242 (2007)

[31] L. Gross: *"A New Human Genome Sequence Paves the Way for Individualized Genomics"*, Public Library of Science Biol. 5(10) e266: 2098-2099 (2007)

[32] H. Haick and D. Cahen: *"Making Contact: Connecting molecules electrically to the macroscopic world"*, Prog. Surf. Sci. 83(4): 217-261 (2008)

[33] W. Haiss et al.: *"Single-Molecule Conductance of Redox Molecules in Electrochemical Scanning Tunneling Microscopy"*, J. Phys. Chem. B 111(24): 6703-6712 (2007)

[34] A. Hassibi, R. Navid, R. W. Dutton and T. H. Lee: *"Comprehensive study of noise processes in electrode electrolyte interfaces"*, J. Appl. Phys. 96(2): 1074-1082 (2004)

[35] J. He, L. Lin, P. Zhang and S. Lindsay: *"Identification of DNA Basepairing via Tunnel-Current Decay"*, Nano Lett. 7(12): 3854-3858 (2007)

[36] J. B. Heng et al.: *"Sizing DNA using a nanometer-diameter pore"*, Biophys. J. 87(4): 2905-2911 (2004)

[37] A. D. Hershey and M. Chase: *"Independent functions of viral protein and nucleic acid in growth of bacteriophage"*, J. Gen. Physiol. 36(1): 39-56 (1952)

[38] H. Hiura, H. Miyazaki and K. Tsukagoshi: *"Determination of the Number of Graphene Layers: Discrete Distribution of the Secondary Electron Intensity Stemming from Individual Graphene Layers"*, Appl. Phys. Exp. 3: 95-101 (2010)

[39] R. W. Holley et al.: *"Structure Of A Ribonucleic Acid"*, Science 147: 1462-1465 (1965)

[40] S. Hong et al.: *"Molecular Conductance Spectroscopy of conjugated, phenol-based molecules on Au(111): the effect of end groups on molecular conduction"*, Superlatti. and Microstruct. 28(4): 289-303 (2000)

[41] P. Y. Huang et al.: *"Grains and grain boundaries in single-layer graphene atomic patchwork quilts"*, Nature 469: 389-392, (2011)

[42] A. P. Ivanov et al.: *"DNA Tunneling Detector Embedded in a Nanopore"*, Nano Lett. 11(1): 279-285 (2011)

[43] A.-P. Jauho, N. S. Wingreen and Y. Meir: *"Time dependent transport in interacting and noninteracting resonant tunneling systems"*, Phys. Rev. B 50(8): 5528-5544 (1994)

[44] J. B. Johnson: *"Thermal Agitation of Electricity in Conductors"*, Phys. Rev. 32(1): 97-109 (1928)

[45] W. K. Johnston, P. J. Unrau, M. S. Lawrence, M. E. Glasner and D. P. Bartel: *"RNA-Catalyzed RNA Polymerization: Accurate and General RNA-Templated Primer Extension"*, Science 292: 1319-1325 (2001)

[46] C. B. Joliffe: *"A study of polarization capacity and resistance at radio frequencies"*, Phys. Rev. 22(3), 293-302 (1923)

[47] R. Kant, R. Kumar and V. K. Yadav *"Theory of Anomalous Diffusion Impedance of Realistic Fractal Electrode"*, J. Phys. Chem. C Lett. 112(11): 4019-4023 (2008)

[48] J.J. Kasianowicz, E. Brandin, D. Branton and D.W. Deamer: *"Characterization of individual polynucleotide molecules using a membrane channel"*, Proc. Natl. Acad. Sci. USA 93(24): 13770-13773 (1996)

[49] U. Keyser et al.: *"Direct force measurements on DNA in a solid-state nanopore"*, Nature Phys. 2: 473-477 (2006)

[50] K. Kim et al.: *"Grain Boundary Mapping in Polycrystalline Graphene"*, ACS Nano 5(3): 2142-2146 (2011)

[51] M. J. Kim, B. McNally, K. Murata and A. Meller: *"Characteristics of solid-state nanometer pores fabricated using a transmission electron microscope"*, Nanotechnology 18(20): 205302 (2007)

[52] M. Krems, M. Zwolak, Y. V. Pershin, M. Di Ventra: *"Effect of Noise on DNA Sequencing via Transverse Electronic Transport"*, Biophys. J. 97(7): 1990-1996 (2009)

[53] J. Kundu et al.: *"Adenine- and Adenosine Monophosphate (AMP)-Gold Binding Interactions Studied by Surface-Enhanced Raman and Infrared Spectroscopies"*, J. Phys. Chem. C 113(32): 14390-14397 (2009)

[54] A. P. Labonte: *"Scanning tunneling spectroscopy on organic molecules"*, PhD Thesis at Purdue University (May 2002)

[55] J. Lagerqvist, M. Zwolak and M. Di Ventra: *"Fast DNA sequencing via transverse electronic transport"*, Nano Lett. 6(4): 779-782 (2006)

[56] J. Lagerqvist, M. Zwolak and M. Di Ventra: *"Comment on characterization of the tunneling conductance across DNA bases"*, Phys. Rev. E. 76(1): 013901 (2007)

[57] J. Lagerqvist, M. Zwolak and M. Di Ventra: *"Influence of the Environment and Probes on Rapid DNA Sequencing via Transverse Electronic Transport"*, Biophys. J. 93(7): 2384-2390 (2007)

[58] J. Lambe and R. C. Jaklevic: *"Molecular Vibration Spectra by Inelastic Electron Tunneling"*, Phys. Rev. 165(3): 821-832 (1968)

[59] S. W. Lee, S. S. Lee and E. H. Yang: *"A Study on Field Emission Characteristics of Planar Graphene Layers Obtained from a Highly Oriented Pyrolyzed Graphite Block"*, Nanoscale Res. Lett. 4(10): 1218-1221 (2009)

[60] P. Levene: *"The structure of yeast nucleic acid"*, J. Biol. Chem. 40(2): 41524 (1919)

[61] G. Li, A. Luican and E. Y. Andrei: *"Scanning Tunneling Spectroscopy of Graphene on Graphite"*, Phys. Rev. Lett 102(17): 176804 (2009)

[62] G. Li et al.: *"Observation of Van Hove singularities in twisted graphene layers"*, Nature Phys. 6: 109-113 (2010)

[63] G. Li and E. Y. Andrei: *"Observation of Landau Levels of Dirac Fermions in Graphite"*, Nature Phy. 3: 623-627 (2007)

[64] J. Li, M. Gershow, D. Stein, E. Brandin and J. A. Golovchenko: *"DNA molecules and configurations in a solid-state nanopore microscope"*, Nature Mat. 2: 611-615 (2003)

[65] X. Li et al.: *"Large-Area Synthesis of High-Quality and Uniform Graphene Films on Copper Foils"*, Science 324: 1312-1314 (2009)

[66] X. Liang and S. Y. Chou: *"Nanogap Detector Inside Nanofluidic Channel for Fast Real-Time Label-Free DNA Analysis"*, Nano Lett. 8(5): 1472-1476 (2008)

[67] H. Liu, Y. Liu and D. Zhu: *"Chemical doping of graphene"*, J. Mater. Chem. 21(10): 3335-3345 (2011)

[68] S. H. Liu et al.: *"Fractal model for the ac response of a rough interface"*, Phys. Rev. Lett. 55(5): 529-532 (1985)

[69] J. T. Long and S. G. Weber: *"Noise at microelectrodes and microelectrode arrays in amperometry and voltammetry"*, Anal. Chem. 60(20): 2309-2311 (1988)

[70] A. Luican et al.: *"Single Layer Behavior and Its Breakdown in Twisted Graphene Layers"*, Phys. Rev. Lett. 106(12): 126802 (2011)

[71] A. K. Mahapatro, S. Ghosh and D. B. Janes: *"Nanometer Scale Electrode Seperation (Nanogap) Using Electromigration at Room Temperature"*, IEEE Transact and Nanotech. 5(3): 232-236 (2006)

[72] T. Maleki, S. Mohammadi and B. Ziaie: *"A nanofluidic channel with embedded transverse nanoelectrodes"*, Nanotechnology 20(10): 105302 (2009)

[73] J. Math, A. Aksimentiev, D. R. Nelson, K. Schulten and A. Meller: *"Orientation discrimination of single stranded DNA inside the alpha hemolysin membrne channel"*, Proc. Natl. Acad. Sci. USA 102(35): 12377-12382 (2005)

[74] A. M. Maxam and W. Gilbert: *"A new method for sequencing DNA."*, Proc. Natl. Acad. Sci. USA 74(2): 560-564 (1977)

[75] E. T. McAdams, A. Lackermeier, J. A. McLaughlin, D. Macken and J. Jossinet: *"The linear and non-linear electrical properties of the electrode-electrolyte interface"*, Biosens. and Bioelec. 10(1-2): 67-74 (1995)

[76] R. L. McCreery: *"Molecular Electronic Junctions"*, Chem. Mater. 16(23): 4477-4496 (2004)

[77] A. Meller, L. Nivon and D. Branton: *"Voltage-driven DNA translocations through a nanopore"*, Phys. Rev. Lett. 86(15): 3435-3438 (2001)

[78] A. Meller, L. Nivon, E. Brandin, J. Golovchenko and D. Branton: *"Rapid nanopore discrimination between single polynucleotide molecules"*, Proc. Natl. Acad. Sci. USA 97(3): 1079-1084 (2000)

[79] C. A. Merchant et al.: *"DNA translocation through Graphene Nanopores"*, Nano Lett. 10(8): 2915-2921 (2010)

[80] D. Meschede: *"Gerthsen Physik"*, Springer, Berlin, 22. edition (August 2003)

[81] S. K. Min, W. Y. Kim, Y. Cho and K. S. Kim *"Fast DNA sequencing with a graphene-based nanochannel device"*, Nature Nanotech. 6, 162165 (2011)

[82] A. Nakabachi et al.: *"The 160-kilobase genome of the bacterial endosymbiont Carsonella"*, Science 314: 267 (2006)

[83] P. Nelson: *"Biologial Physics"*, W. H. Freeman and Company; Madison Avenue, New York, 1st edition (July 18, 2003)

[84] T. Nelson, B. Zhang and O. V. Prezhdo: *"Detection of Nucleic Acids with Graphene Nanopores: Ab Initio Characterization of a Novel Sequencing Device"*, Nano Lett. 10(9): 3237-3242 (2010)

[85] M. W. Nirenberg and J. H. Matthaei: *"The Dependence Of Cell- Free Protein Synthesis In E. coli Upon Naturally Occurring Or Synthetic Polyribonucleotides"*, Proc. Natl. Acad. Sci. USA 47(10): 1588-1602 (1961)

[86] M. W. Nirenberg et al.: *"RNA codewords and protein synthesis, VII. On the general nature of the RNA code"*, Proc. Natl. Acad. Sci. USA 53(5): 1161-1168 (1965)

[87] A. Nitzan: *"A relationship between electron-transfer rates and molecular conduction"*, J. Phys. Chem. A 105(12): 2677-2679 (2001)

[88] A. Nitzan: *"Electron transmission through molecules and molecular interfaces"*, Annu. Rev. Phys. Chem. 52: 681-750 (2001)

[89] K. S. Novoselov et al.: *"Electric Field Effect in Atomically Thin Carbon Films"*, Science 306: 666-669 (2004)

[90] H. Nyquist: *"Thermal Agitation of Electric Charge in Conductors"*, Phys. Rev. 32(1): 110-113 (1928)

[91] J. Oomens et al.: *"The Ethylene Hot Band Spectrum near 3000cm^{-1} "*, J. Mol. Spect. 180(2): 236-248 (1996)

[92] H. Park et al.: *"Nanomechanical oscillations in a single-C60 transistor"*, Nature 407: 57-59 (2000)

[93] J. Park: *"Electron Transport in Single Molecule Transistors"*, PhD Thesis Advisor: Paul L. McEuen, University of California Berkeley (2003)

[94] H. W. C. Postma: *"Rapid Sequencing of Individual DNA Molecules in Graphene Nanogaps"*, Nano Lett. 10(2): 420-425 (2010)

[95] J. Prasongkit, A. Grigoriev, B. Pathak, R. Ahuja and R. H. Scheicher: *"Transverse conductance of DNA nucleotides in a graphene nanogap from first principles"*, Nano Lett. 11(5): 1941-1945 (2011)

[96] N. Prokopuk, K.-a. Son and C. Waltz: *"Electron Tunneling through Fluid Solvents"*, J. Phys. Chem. C 111(17): 6533-6537 (2007)

[97] W. Regan et al.: *"A direct transfer of layer-area graphene"*, Appl. Phys. Lett. 96(11): 113102 (2010)

[98] A. Reiner et al.: *"Large Area, Few-Layer Graphene Films on Arbitrary Substrates by Chemical Vapor Deposition"*, Nano Lett. 9(1): 30-35 (2009)

[99] W. Reisner et al.: *"Statics and Dynamics of Single DNA Molecules Confined in Nanochannels"*, Phys. Rev. Lett. 94(19): 196101 (2005)

[100] J. Repp, G. Meyer, S. M. Stojkovi, A. Gourdon and C. Joachim: *"Molecules on Insulating Films: Scanning-Tunneling Microscopy Imaging of Individual Molecular Orbitals"*, Phys. Rev. Lett. 94(2): 026803 (2005)

[101] R. M. Ribeiro, V. M Pereira, N. M. R. Peres, P. R. Briddon and A. H. C. Neto: *"Strained graphene: tight-binding and density functional calculations"*, New J. Phys. 11: 115002 (2009)

[102] A. Rochefort, M. Di Ventra and P. Avouris: *"Switching behavior of semiconducting carbon nanotubes under an external electric field"*, Appl. Phys. Lett. 78(17): 2521 (2001)

[103] D. A. Ryndyk et al.: *"Scanning Tunneling Spectroscopy of Single DNA Molecules"*, ACS Nano 3(7): 1651-1656 (2009)

[104] G. B. Salieb-Beugelaar et al.: *"Field-Dependent DNA Mobility in 20 nm High Nanoslits"*, Nano Lett. 8(7): 1785-1790 (2008)

[105] F. Sanger and A. R. Coulson: *"A rapid method for determining sequences in DNA by primed synthesis with DNA polymerase"*, J. Mol. Biol. 94(3): 441-446 (1975)

[106] F. Sanger, S. Nicklen and A. R. Coulson: *"DNA sequencing with chain-terminating inhibitors"*, Proc. Natl. Acad. Sci. USA 74(12): 5463-5467 (1977)

[107] G. Schneider et al.: *"DNA translocation through Graphene Nanopores"*, Nano Lett. 10(8): 3163-3167 (2010)

[108] Y. Selzer and D. L. Allara: *"Single-molecule electrical junctions"*, Annu. Rev. Phys. Chem. 57:593623 (2006)

[109] Y. J. Shin et al.: *"Tunneling characteristics of graphene"*, Appl. Phys. Lett. 97(25): 252102 (2010)

[110] J. G. Simmons: *"Generalized Formula for the Electric Tunnel Effect between Similar Electrodes Separated by a Thin Insulating Film"*, J. Appl. Phys. 34(6): 1793 (1963)

[111] H. Song et al.: *"Vibrational spectra of metal-molecule-metal junctions in electromigrated nanogap electrodes by inelastic electron tunneling"*, Appl. Phys. Lett. 94(10): 103-110 (2009)

[112] W. Sparreboom, J. C. T. Eijkel, J. Bomer and A. van den Berg: *"Rapid sacrificial layer etching for the fabrication of nanochannels with integrated metal electrodes"*, Lab Chip 8: 402-407 (2008)

[113] R. Stadler, K. W. Jacobsen: *"Fermi level alignment in molecular nanojunctions and its relation to charge transfer"*, Phys. Rev. B 74(16), 161405(R) (2006)

[114] A. J. Storm et al.: *"Fast DNA translocation through a solid-state nanopore"*, Nano Lett. 5(7): 1193-1197 (2005)

[115] D. R. Strachan et al.: *"Controlled fabrication of nanogaps in ambient environment for molecular electronics"*, Appl. Phys. Lett. 86(4): 043109 (2005)

[116] D. R. Strachan et al.: *"Clean Electromigrated Nanogaps Imaged by Transmission Electron Microscopy"*, Nano Lett. 6(3): 441-444 (2006)

[117] K. Suenaga and M. Koshino: *"Atom-by-atom spectroscopy at graphene edge"*, Nature 468: 1088-1090 (2010)

[118] N. J. Tao: *"Electron transport in molecular junctions"*, Nature Nanotech. 1: 173-181 (2006)

[119] J. Tegenfeldt et al.: *"The dynamics of genomic-length DNA molecules in 100-nm channels"*, Proc. Natl Acad. Sci. USA 101(30): 10979-10983 (2004)

[120] L. H. Thamdrup, A. Klukowska and A. Kristensen: *"Stretching DNA in polymer nanochannels fabricated by thermal imprint in PMMA"*, Nanotechnology 19: 125301 (2008)

[121] W. Tieng et al.: *"Conductance spectra of molecular wires"*, J. Chem. Phys. 109(7): 2874-2882 (1998)

[122] M. Tsutsui, M. Taniguchi, K. Yokota and T. Kawai: *"Identifying single nucleotides by tunneling current"*, Nature Nanotech. 5: 286-290 (2010)

[123] H. S. J. van der Zant, E. A. Osorio, M. Poot and K. ONeill: *"Electromigrated molecular junctions"*, Phys. Stat. Sol. (b) 243(13): 3408-3412 (2006)

[124] K. V. Voelkerding, S. A. Dames and J. D. Durtschi: *"Next Generation Sequencing: From Basic Research to Diagnostics"*, Clin. Chem. 55(4): 41-47 (2009)

[125] V. N. Votov: *"Electron-Electron Interactions in Graphene: Current Status and Perspectives"*, Submitted to Reviews of Modern Physics; http://arxiv.org/abs/1012.3484 (2010)

[126] W. Xuan, Z. Linjie, and K. Müllen: *"Transparent, Conductive Graphene Electrodes for Dye-Sensitized Solar Cells"*, Nano Lett. 8(1): 323-327 (2008)

[127] E. Warburg: *"Über die Polarisationscapacität des Platins"*, Annalen der Physik 311(9): 125-135 (1901)

[128] M. Wanunu, J. Sutin and A. Meller: *"DNA Profiling Using Solid-State Nanopores: Detection of DNA-Binding Molecules"*, Nano Lett. 9(10): 3498-3502 (2009)

[129] M. Wanunu et al.: *"Rapid Electronic Detection of Probe-Specific MicroRNAs Using Thin Nanopore Sensors"*, Nature Nanotech. 5: 807-814 (2010)

[130] M. Wanunu et al.: *"Discrimination of methylcytosine from hydroxymethylcytosine in individual DNA Molecules"*, J. Am. Chem. Soc. 133(3): 486-492 (2011)

[131] J. D. Watson and F. H. C. Crick: *"A Structure for Deoxyribose Nucleic Acid"*, Nature 171: 737738 (1953)

[132] S. G. Weber et al.: *"Signal-to-noise ratio in microelectrode-array-based electrochemical detectors"*, Anal. Chem. 61(4): 295-302 (1989)

[133] R. Wiesendanger: *"Scanning Probe Microscopy"*, Cambridge University Press (November 25, 1994)

[134] J. Yeager et al.: *"Low Level Measurements"*, 5th Edition, Keithley Instruments, Cleveland (1993)

[135] H. Yuhui et al.: *"Enhanced DNA sequencing performance through edge-hydrogenation of graphene electrodes"*, accepted for publication in Adv. Funct. Mater. 2011; http://arxiv.org/abs/1012.0031 (2011)

[136] M. Zwolak and M. Di Ventra: *"Electronic Signature of DNA Nucleotides via Transverse Transport"*, Nano Lett. 5(3): 421-424 (2005)

[137] M. Zwolak and M. Di Ventra: *"Colloquium: Physical approaches to DNA sequencing and detection"*, Rev. Mod. Phys. 80(1): 141-165 (2008)

Vita

Manuel Schottdorf

2007-2010 B. Sc. in Physics from the University of Würzburg, Degree 1.2 "excellent". Thesis "Nanofluidic Microelectrode Array as cell/chip interface"

2007 Graduated from High School "Frobenius Gymnasium" in Hammelburg, Germany, degree "1.9"

2009-2010 Teaching assistant for "Computational Physics", Department of Physics, University of Würzburg